PRECLINICAL EFFICACY OF AN EPICARDIAL HEART ASSIST DEVICE

A Dissertation

by

ERICA CHRISTINE HORD

Submitted to the Office of Graduate and Professional Studies of
Texas A&M University
in partial fulfillment of the requirements for the degree of

DOCTOR OF PHILOSOPHY

Chair of Committee,	John C. Criscione
Committee Members,	Michael R. Moreno
	Christopher M. Quick
	Egemen Tuzun
Head of Department,	Anthony Guiseppi-Elie

May 2017

Major Subject: Biomedical Engineering

ABSTRACT

Of the millions of Americans with heart failure, a significant portion are end-stage and experience symptoms even at rest. Moreover, around half of people with heart failure die within 5 years of diagnosis. The ideal treatment option for these patients is a heart transplant. However, fewer than 3000 donor hearts are available for transplant in North America each year. Given the significant disparity in number of donor hearts and end-stage failure patients, there is great clinical need for heart assist technology that supports heart function, and for improved approaches that lead to heart recovery.

The current leading device therapy for advanced heart failure patients is a Ventricular Assist Device (VAD). While these devices have been clinically available in the United States since 2003, they are associated with severe complications – including a high risk for stroke and gastrointestinal bleeding. As an alternative to mechanical blood pumps, direct cardiac compression (DCC) devices have been developed for heart assist. The investigation described herein includes the development, simulation, and preclinical testing of a novel DCC device – coined the EpicHeart™ (Epicardial Heart Assist Device).

First, engineering design improvements were required to allow for synchronization between device activation and the native contraction of the heart. The methods to accomplish this goal are described with results of *in vivo* testing. Then, the hemodynamic effects of the device in an acute heart failure model were investigated. Finally, the results of the *in vivo* testing of the device were applied for technical specification verification of a simulation platform developed to model the clinical effects of the EpicHeart™ Device.

The outcomes of this study have yielded an improved preclinical medical device that will proceed with future investigations over longer study durations as well as other heart failure etiologies – while continuing to explore potential for heart recovery. Additionally, the pilot study of simulating this technology is unique and has provided support for future validation of a clinical simulation tool. This simulation is anticipated for use in a clinical environment to predict patient outcomes of the EpicHeart™ Device for treatment of heart disease.

DEDICATION

This work is dedicated to my family, especially my parents Rick and Michele Hord. Together you have inspired me to want to make a difference in medicine, and have always encouraged my scientific curiosity. I am grateful for all that you have done to support my engineering education, and my career as a professional student.

To my siblings, Megan, Natalie, Krista, and Ricky, I am thankful for your comic relief, and admittedly a little friendly competition that always pushes us to achieve more. I am proud of all of you.

Finally, thank you to all of my grandparents. You have taught us to work hard for what we want in life, and I am thankful for all that I have learned from you. I wish you were all still here to see this work completed. I love and miss you.

ACKNOWLEDGEMENTS

First and foremost, I would like to thank my committee members for their contributions and guidance. Thank you to Dr. Moreno and Dr. Quick for what I have learned during my graduate courses, and for your guidance in my research. Thank you to Dr. Tuzun for your continued support and everything you have taught me about preclinical studies. Thank you to Dr. Bolch for your friendship and mentorship. Finally, thank you to Dr. Criscione for giving me the opportunity to work under your guidance. I am so grateful for how much I have learned from you over the past five years.

I would also like to thank the staff members at the Texas A&M Institute for Preclinical Studies and the Texas Heart Institute for your contributions to our studies. Additionally, thank you to the CorInnova employees and Dr. Daniel Burkhoff for your support of this work.

Finally, I cannot say thank you enough to my friends Megan, Jessi, Nichole, Nicole, Amanda, Andrea, Briana, and Elyse for your support throughout my nine-year career as a professional student. I would not have made it without you.

CONTRIBUTORS AND FUNDING SOURCES

Contributors

This work was supervised by a dissertation committee consisting of Dr. John C. Criscione, Dr. Michael R. Moreno, and Dr. Egemen Tuzun of the Biomedical Engineering Department, Professor Christopher M. Quick of the Department of Veterinary Physiology and Pharmacology, and Dr. Christina M. Bolch, Senior Biomedical Engineer of CorInnova, Incorporated.

The simulation outputs used for analysis in Section III were compiled by Reagan Tompkins of the Biomedical Engineering Department, and the simulation application was provided by Dr. Daniel Burkhoff of the Cardiovascular Research Foundation.

All other work conducted for the dissertation was completed by the student, in collaboration with CorInnova, Incorporated.

Funding Sources

Graduate study was supported by a fellowship from the Texas A&M Engineering Experiment Station, a teaching fellowship from the Texas A&M University Biomedical Engineering Department, and through an internship with CorInnova, Incorporated. This work was funded by The Wellcome Trust, Translation Fund Award no. 104613, awarded to CorInnova, Incorporated. The contents of this document are solely the responsibility of the authors and do not necessarily represent the official views of The Wellcome Trust.

NOMENCLATURE

AoP	Aortic Pressure
BPM	Beats Per Minute
CO	Cardiac Output
CRI	Continuous Rate of Infusion
CVP	Central Venous Pressure
DBP	Diastolic Blood Pressure
ECG	Electrocardiogram
ED	End-Diastolic
EDP	End-Diastolic Pressure
EDPVR	End-Diastolic Pressure Volume Relationship
EDV	End-Diastolic Volume
EHI	EpicHeart™ Implantable
EHDP	EpicHeart™ Device Pressure
EF	Ejection Fraction
ES	End-Systolic
ESP	End-Systolic Pressure
ESPVR	End-Systolic Pressure Volume Relationship
ESV	End-Systolic Volume
HR	Heart Rate
IABP	Intra-Aortic Balloon Pump

LV	Left Ventricle
LVSW	Left Ventricular Stroke Work
LVSV	Left Ventricular Stroke Volume
LVP	Left Ventricular Pressure
MAP	Mean Arterial Pressure
PADP	Pulmonary Artery Diastolic Pressure
PAMP	Pulmonary Artery Mean Pressure
PASP	Pulmonary Artery Systolic Pressure
PV	Pressure-Volume
RV	Right Ventricle
SBP	Systolic Blood Pressure
SV	Stroke Volume
SW	Stroke Work
VAD	Ventricular Assist Device

TABLE OF CONTENTS

Page

LIST OF FIGURES

Page

LIST OF TABLES

Page

1. INTRODUCTION: THE NEED FOR HEART FAILURE THERAPY

1.1. Heart Failure: Prevalence, Cost, and Pathology

Heart failure (HF) is a chronic, progressive condition in which the pumping capacity of the heart has declined to a point where it cannot meet the blood and oxygen demands of the body. This condition is a major public health issue, with over 6.5 million Americans currently living with HF, and 960,000 new cases diagnosed annually.[1] Moreover, it is projected that the prevalence of HF will increase by 46% from 2012 to 2030, resulting in more than 8 million adults with HF.[1] In addition to the high incidence rate, the prognosis of heart failure is poor; approximately 50% of people diagnosed with heart failure will die within 5 years.[1] The annual mortality where heart failure was the underlying cause was over 68,000 in 2014, with the number of any-mention deaths attributable to HF at 309,000.[1] From a financial standpoint, economic reports estimate that the total cost was $30.7 billion in 2012, with 68% of the total attributable to direct medical costs.[1] Moreover, projections show that by 2030, the total cost of HF will increase almost 127% to $69.7 billion.[1]

The development of this condition is usually initiated by a specific cardiac event, such as myocardial infarction, that causes a reduction in the contractile strength of the heart. The heart compensates for its weakened state by Frank-Starling mechanisms as a result of renin-angiotensin retention of salt and water by the kidneys to increase total blood volume. However, the increase in hydrostatic pressure impairs venous return to the heart,

further increasing the load on the heart. Eventually, the ventricles begin to dilate in order to relieve abnormal mechanical stresses. This pathological remodeling process results in a significantly reduced ventricular wall thickness with myocyte slippage, and an increase in the end-diastolic volume of the ventricle. The dilated ventricle becomes more spherical in geometry, and combined with the thinning wall, the wall stress is significantly increased, culminating in a condition known as dilated cardiomyopathy.[2-6]

Current pharmacological therapies, such as ACEIs and β-Blockers, used to symptomatically treat HF have a significant positive effect on morbidity and mortality.[7] However, these drug regimens fail to address the remodeling tissue, and eventually lose efficacy. Surgery is not commonly used for early HF treatment, unless a correctable problem can be identified, such as aortic stenosis, mitral valve regurgitation, or coronary artery occlusion. In cases of post-myocardial infarction, the tissue necrosis extends beyond the infarcted area, and cannot be remedied via surgical methods.

As the condition progresses beyond the help of drug therapy, the patient reaches end-stage heart failure, a state at which the patient experiences symptoms even while at rest.

1.2. Ideal Treatment: Heart Transplant

The ideal treatment for end-stage HF patients is a heart transplant, with a 11-year median survival after receiving a new heart.[8] However, fewer than 3,000 transplants are performed annually in North America.[8] Additionally, transplant recipients are limited by multiple contraindications disqualifying a patient from receiving a donor heart.[9] Those

patients who receive a heart transplant must be prescribed life-long immunosuppressant drugs, and are at risk for complications such as organ rejection and transplant coronary allograft vasculopathy. Given the significant disparity in available donor hearts and patients in need, an alternative therapy is required.

2. EVALUATION OF THE EPICHEART™ ASSIST DEVICE IN AN ACUTE HEART FAILURE MODEL

While it is expected that the most dramatic effects from the EpicHeart™ Device will be observed in chronic heart failure subjects, further testing in the acute stages is necessary to refine the designs, explore possible indications for use, and examine the potential conditions for optimal heart assist. This section describes the results of *in vivo* device testing in an ovine acute HF model.

2.1. Introduction

Of the 6.5 million Americans with heart failure, a significant portion are end-stage and experience symptoms even at rest.[1] The ideal treatment option for these patients is a heart transplant, with a 11-year median survival after receiving a new heart.[8] However, fewer than 3,000 donor hearts are available for transplant in North America each year.[8] Given the significant disparity in number of donor hearts and end-stage failure patients, there is great clinical need for heart assist technology that supports heart function, and for improved approaches that lead to heart recovery. As discussed by Moreno et al and advanced in the recent study by Roche et al, a properly designed direct cardiac compression (DCC) device that corrects aberrant heart motions and enhances heart contractility may be able to provide both heart assist and a potential means to enable heart recovery—provided that proper deformation of myocardium is needed for heart tissue growth and remodeling.[10-12]

The results in the Moreno single animal studies demonstrate the possibility of restoring proper cardiac kinematics with a soft DCC implanted through a less invasive procedure than standard open heart surgery.[10,11] This report furthers this work with design improvements (eliminating the need for guidewires in the deployment) and with multiple studies in an ovine model of acute heart failure (5 sheep with esmolol overdose).

2.2. Materials and Methods

2.2.1. EpicHeart™ Cardiac Assist Device

The EpicHeart™ is a cardiac assist device that applies direct cardiac compression to the outside of the heart (epicardium) in synchrony with systole. The method of cardiac assist employed by the EpicHeart™ Implantable (EHI) is a unique combination of "active" assist, applied during systole with air infused into multiple bladders connected together in the form of a cup shape, in conjunction with a "passive" component that is in direct contact with the epicardium.[13] The passive component consists of fluid-filled bladders that accommodate any gaps in the interface between the device and heart, while also enabling the heart to twist relative to the active component during contraction. All chambers of the EHI are constructed from thin-film thermoplastic polyurethane material. The EHI is supported by a superelastic Nitinol wire frame, and is compressed into a cylinder (deployment tube) for minimally invasive deployment around the heart. See Figure 1 for fluoroscopic images showing the EHI implanted about the heart with contrast media in the passive chamber and air in the active component.

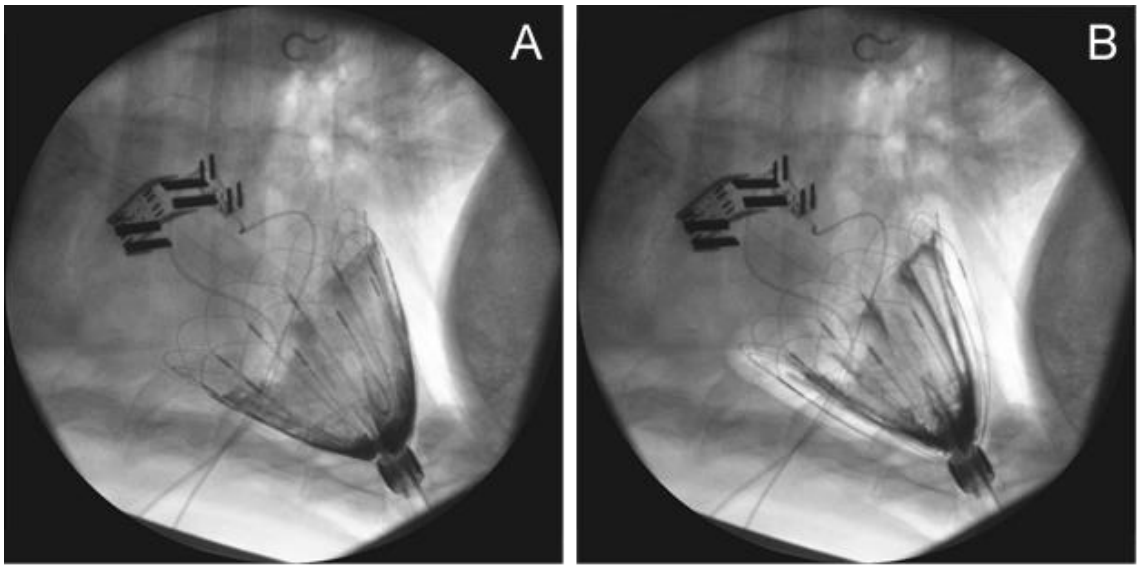

Figure 1. Fluoroscopic images of the EHI during standby (A), and during systolic assist (B); imaging contrast media was used as the fluid in the passive chambers for visual aid (darkest regions)

The EHI was operated using a custom programmable drive system – henceforth referred to as the Driver. The ovine ECG was acquired using epicardial electrodes, and was gated by a custom-gain cardiac trigger monitor (Model 7700, IVY Biomedical). Using a custom programmable controller, the gated ECG signal is used to trigger the activation of solenoid valves, which were tailored to modulate the pressure of the active chambers in synchrony with systole. A Millar Mikro-Tip® Catheter Pressure Transducer (Model SPR-320, Size 2F) was used to measure the fluid pressure in the passive chambers, providing a metric of epicardial assist pressure. The EHI was activated for short periods of time (<5min) during this study with intermittent periods of device standby to observe the acute effects of EHI assist.

2.2.2. Study Design and Surgical Procedure

Five (5) separate acute ovine, non-GLP studies were conducted for this investigation. All experiments were conducted under an Animal Use Protocol (AUP) that was approved by the Texas A&M University Institutional Animal Care and Use Committee (IACUC) or the Texas Heart Institute IACUC. Each study utilized a single, anesthetized adult domestic cross ovine (50-78 kg). Upon induction of anesthesia, catheters were placed to facilitate the administration of medications as well as for monitoring of vital parameters. AoP and LVP were monitored by either fluid-filled catheters or a Millar Mikro-Tip® Catheter Dual Pressure Transducer (SPR-751) placed across the aortic valve. A Swan-Ganz (Edwards Lifesciences) catheter was used to measure the CVP and PAP. A left-thoracotomy was performed to expose the aorta, without opening the pericardium, and a Transonic COnfidence Flowprobe® was placed around the ascending aorta to monitor CO before closing the incision.

An apical approach was achieved through a subxyphoid incision with xyphoidectomy. After performing the xyphoidectomy, the surgeon opened a small (approximately 1 in. diameter) circular incision at the pericardial apex, and then constructed a pericardial cradle to stabilize the pericardial edges. A pericardiogram was performed for imaging of the epicardial structures by infusing contrast media directly into the pericardial sac through the apical hole.[14] Prior to deployment, the EHI was loaded into a deployment tube (PTFE 2.5 cm OD, 2.3 cm ID, 20 cm Length), with radiopaque marker tape used to visualize the distal end of the tube under fluoroscopic imaging (Indicator® 1.0mm Lines – IZI Medical Products). To prepare for implantation, the deployment tube

was placed inside the pericardial sac to align the fluoroscopy C-arm with the plane of the device; the radiopaque indicator lines provided a reference for the plane, with proper positioning defined as a field of view normal to the deployment tube. The EHI was then advanced from the deployment tube around the heart under fluoroscopic guidance, inside the pericardium (Figure 2). Once the EHI was in place around the heart (with positioning verified by fluoroscopy), the deployment tube was retracted, and the pneumatic driveline was tunneled to exit through the sternal incision before closing. After removing air in the chest via a chest tube, the passive chamber of EHI was filled with an appropriate volume of imaging contrast media such that the peak pressure measured in the passive chambers during device standby reflected the ventricular end-diastolic pressure. Finally, after filling the passive chamber and connecting the epicardial electrodes, assist was initiated at a low pressure to confirm stable ECG gating. The amount of assist was increased until no adverse effects of additional air infusion were observed, such as pre-ventricular contractions (PVC).

A high dose of esmolol was utilized to model acute heart failure. In addition to creating a stable, dose-dependent failure, esmolol has the benefit of rapid metabolism with a clearance half-life of only 9 min – allowing for rapid return to the baseline state.[15] After all measurements were collected during the animal's baseline state, an appropriate combination of bolus (20-150 mg) and continuous rate of infusion (CRI) (10-300 mL/hr, [10mg/mL]) was administered to target a 50% reduction in CO. The dose varied with each animal, and was managed by the animal anesthesia staff.

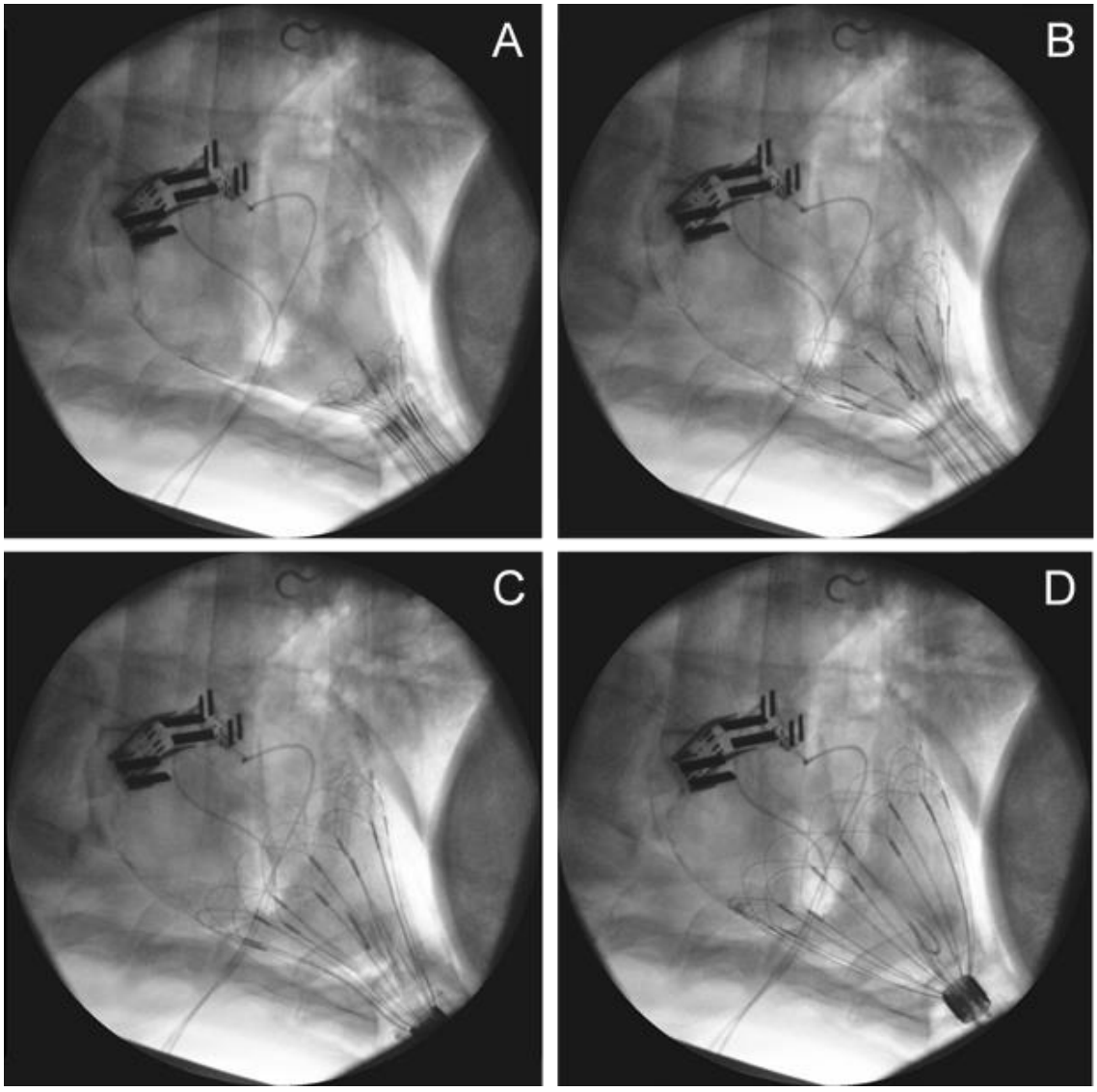

Figure 2. Fluoroscopic imaging of minimally invasive deployment of the EHI; initial advancement from the deployment tube, inside the apex of the pericardium (A), progressive stages of deployment (B, C), and the EHI in place around the heart, inside the pericardium (D)

2.2.3. Data Collection and Statistical Analysis

ADInstruments PowerLab data acquisition hardware and LabChart software were used to continuously record all physiologic parameters and EpicHeart™ Device data. Paired samples of 20 seconds of device standby and successive device assist were collected for analysis. A data inclusion criteria of 20% ≥ CO ≥ 60% reduction from baseline was implemented to filter samples considered outside the targeted failure state. The data population over all 5 animals consisted of 62 paired samples of 20s of data (mean n = 29 ± 3 cardiac cycles per 20s sample). The samples were averaged over the 20s selection using LabChart, and then averaged in Microsoft Excel to provide an overall effect for each animal. Standard deviations are representative of variations amongst data runs for each animal—i.e., each run included a 20s sample of standby paired with a 20s sample of assist immediately following standby. A two-tailed, paired t-test was used for comparison between device standby and assist for each animal, with an alpha level of 0.05 (Excel).

2.3. Results

2.3.1. Deployment

Minimally invasive deployment was successful and uneventful on the first attempt for four out of the five studies, and was successful on the second attempt for the remaining study. In each case, EHI placement was completed without the need for cardiopulmonary bypass, with some brief disruption of normal cardiac electrical conduction and contraction. Electrical conduction returned to normal sinus rhythm once deployment was

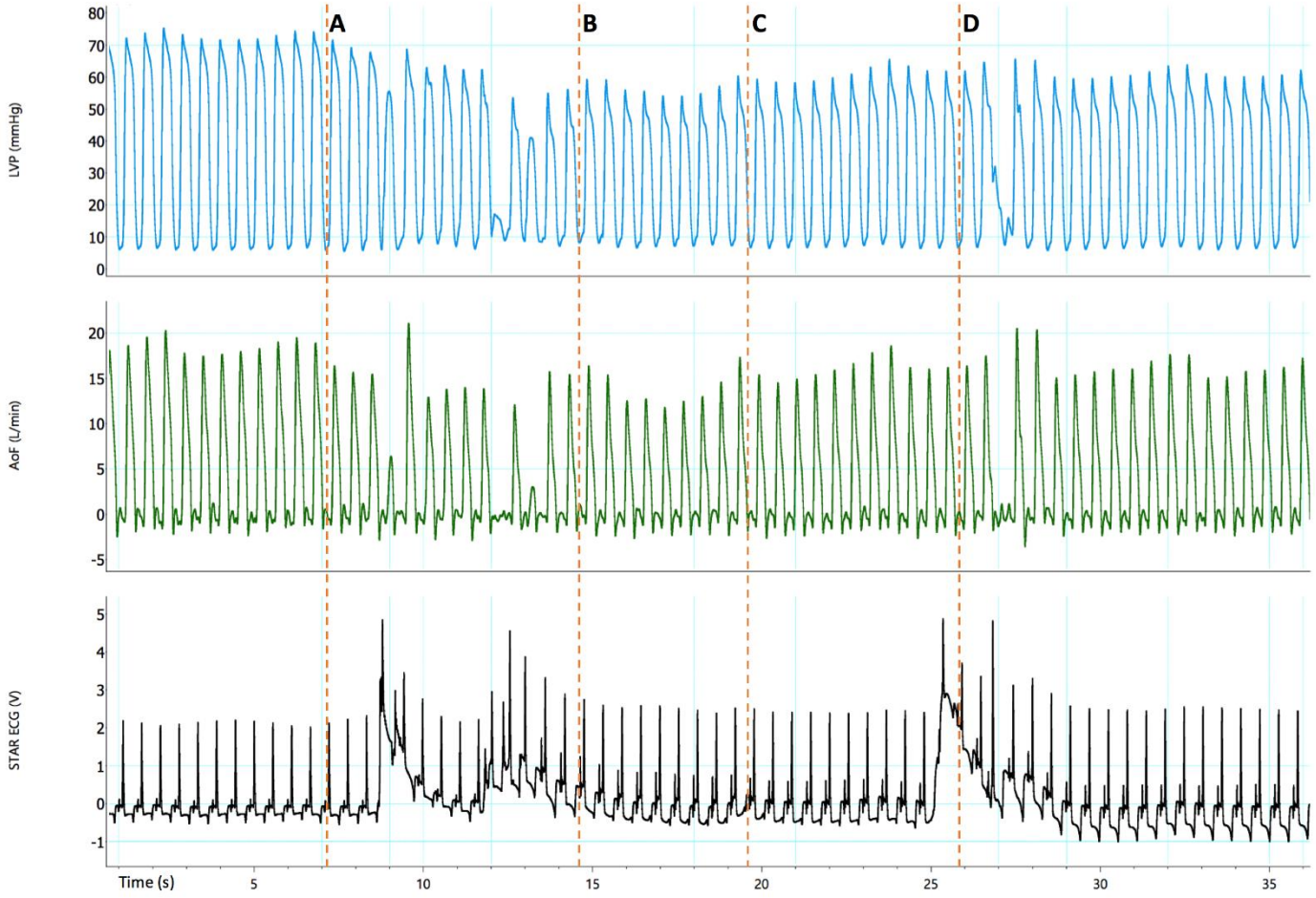

Figure 3. Representative waveforms showing the off-pump EHI placement; (A) designates the start of deployment, (B) the end of deployment, (C) the timing of deployment tube removal, and (D) is the final positioning of the EHI and driveline prior to closing the chest; data sampled from Study 4

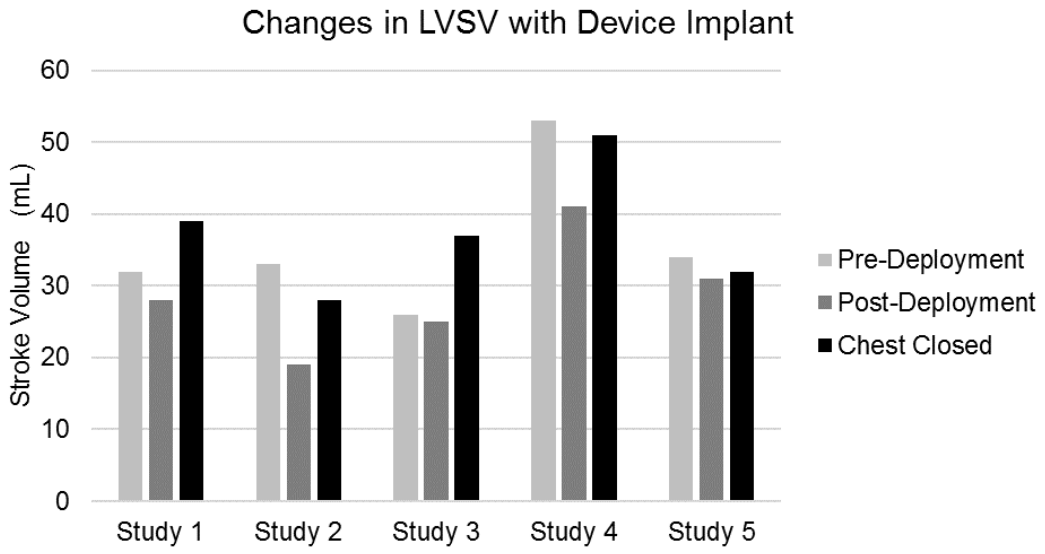

Figure 4. Changes in LVSV with device implant; the pre- and post- deployment time points were sampled immediately before and after deploying the EHI, and steady state samples were taken after closing the chest; notice that some depression occurs immediately upon implant, however recovers after reaching steady state in all cases

complete. Figure 3 is representative data demonstrating the hemodynamics during deployment. EHI placement time after initial advancement to removal of deployment tube was on average less than 25 seconds. Figure 2 shows the minimally invasive deployment process.

With each animal, some depression of cardiac function occurred immediately following deployment. Overall, the CO decreased by 0.7 ± 0.5 L/min immediately post-deployment, however, it then recovered by 0.7 ± 1.1 L/min following chest closure and achievement of steady state. Similarly, the LVSV decreased by 7 ± 6 mL, then recovered by 9 ± 4 mL (108% recovered). Additionally, the MAP decreased by 16 ± 16 mmHg immediately post-deployment, then recovered by 12 ± 20 mmHg. These changes in

hemodynamic parameters (SV and MAP) are plotted for each study in Figure 4 and Figure 5.

Other hemodynamic parameters showed minimal affect from EHI deployment. The average pulmonary artery mean pressure (PAMP) across all studies showed no change with deployment, and increased by 2 ± 2 mmHg once the chest was closed. Additionally, the mean CVP increased by 1 ± 1 mmHg upon deployment and remained the same after chest closure (0 ± 2 mmHg). Lastly, although the LV EDP showed varied effects with deployment, the overall change with deployment was an increase of 2 ± 1 mmHg, and an increase of 2 ± 4 mmHg after reaching steady state.

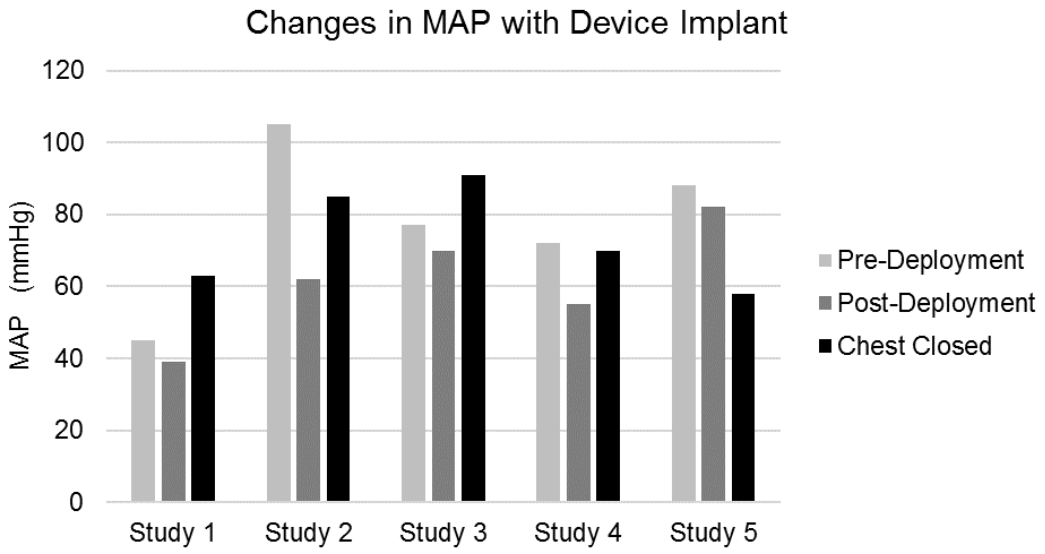

Figure 5. Changes in MAP with device implant; the pre- and post- deployment time points were sampled immediately before and after deploying the EHI, and steady state samples were taken after closing the chest; notice that some depression occurs immediately upon implant, however recovers after reaching steady state; the exception is Study 5, where procainamide was used to lower the HR

Table 1. Mean Failure State Hemodynamic Data. Summary of mean hemodynamic data during esmolol failure state for each acute ovine study; the sample size indicates the number of samples for the given study; each sample was 20 seconds of cardiac cycles

	CO	**SBP**	**DBP**	**MAP**	**LVP**	**CVP**	**PASP**	**PADP**	**PAMP**	**LV EDP**	**LV SW**	**Sample**
	L/min	mmHg	mmHg	mmHg	mmHg	mmHg	mmHg	mmHg	mmHg	mmHg	mmHg*mL	**Size**
STUDY 1	*2.4*	*49*	*30*	*37*	*47*	*12*	*21*	*14*	*17*	*14*	*1110*	*n=13*
STUDY 2	*1.8*	*59*	*38*	*48*	*49*	*12*	*21*	*13*	*16*	*14*	*1138*	*n=14*
STUDY 3	*2.1*	*56*	*37*	*44*	*54*	*12*	*26*	*9*	*18*	*16*	*1156*	*n=20*
STUDY 4	*2.2*	*47*	*27*	*35*	*39*	*17*	*N/A*	*N/A*	*N/A*	*12*	*976*	*n=3*
STUDY 5	*1.9*	*56*	*39*	*47*	*58*	*12*	*N/A*	*N/A*	*N/A*	*19*	*1196*	*n=12*
AVERAGE	***2.1***	***53***	***34***	***42***	***49***	***13***	***23***	***12***	***17***	***15***	***1115***	

2.3.2. Acute Failure Assist

Upon activating the EHI on the failed heart, several hemodynamic parameters showed trends of marked improvement with systolic assist. The failure state hemodynamic data prior to assist is summarized in Table 1, and the average changes with assist are summarized in Table 2. In terms of recovering the healthy baseline prior to esmolol failure state, device assist recovered the CO by an average of 75% and the LVSW by 71% (mean of all 5 studies). This recovery of baseline CO is plotted in Figure 6 for each study. Figure 7 shows representative hemodynamic waveforms of device standby and assist during failure state.

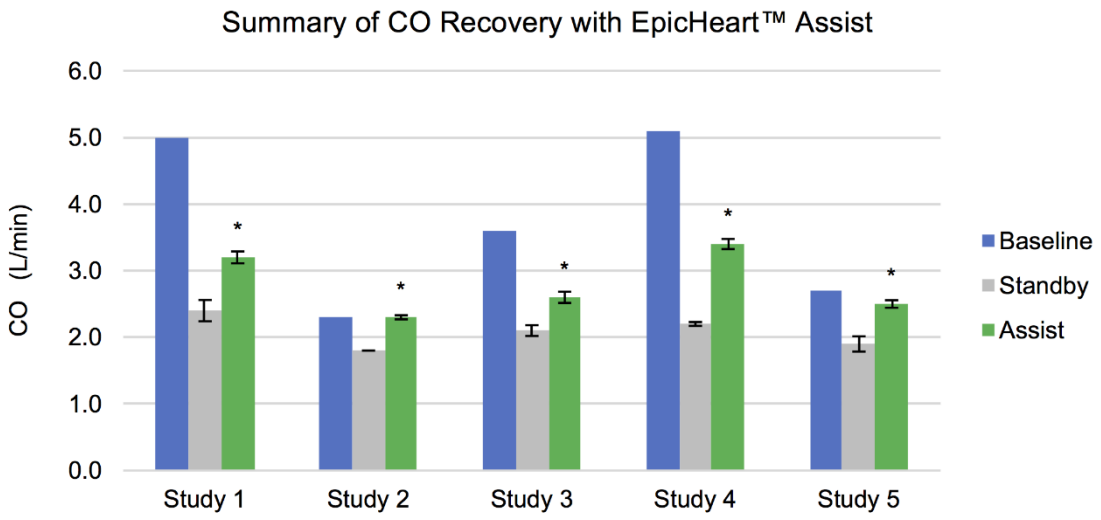

Figure 6. Summary of changes in CO for each study; the Baseline data reflects the CO sampled just prior to inducing esmolol failure, Standby represents the mean CO during failure without device assist, and Assist shows the new CO during periods of device activation; the overall average recovery of CO was 75%.
p < 0.01

Table 2. Changes in Mean Hemodynamics with Assist. Summary of mean hemodynamic changes with device assist during esmolol failure for each acute ovine study; the sample size indicates the number of paired Standby-Assist samples of device action for the given study; each sample was 20 seconds of cardiac cycles

	ΔCO	**ΔSBP**	**ΔDBP**	**ΔMAP**	**ΔLVP**	**ΔCVP**	**ΔPASP**	**ΔPADP**	**ΔPAMP**	**ΔLVEDP**	**ΔLVSW**	**Sample**	**Assist**
	L/min	mmHg	mmHg	mmHg	mmHg	mmHg	mmHg	mmHg	mmHg	mmHg	mmHg*mL	**Size**	mmHg
STUDY 1	*0.8*	*12*	*3*	*6*	*14*	*0*	*2*	*-1*	*0*	*0*	*859*	*n=13*	*12*
STUDY 2	*0.5*	*13*	*4*	*5*	*13*	*1*	*9*	*-1*	*2*	*0*	*680*	*n=14*	*8*
STUDY 3	*0.5*	*12*	*-4*	*8*	*13*	*-3*	*13*	*-8*	*4*	*0*	*696*	*n=20*	*19*
STUDY 4	*1.2*	*12*	*1*	*6*	*11*	*-1*	*N/A*	*N/A*	*N/A*	*0*	*764*	*n=3*	*10*
STUDY 5	*0.6*	*14*	*3*	*7*	*14*	*0*	*N/A*	*N/A*	*N/A*	*-2*	*811*	*n=12*	*16*
AVERAGE	***0.7***	***13***	***1***	***6***	***13***	***-1***	***8***	***-3***	***2***	***0***	***762***		

Overall, the CO improved by 0.7 ± 0.3 L/min (+34%), SBP improved by 13 ± 1 mmHg, and pulmonary artery systolic pressure (PASP) improved by 8 ± 5 mmHg. Similarly, the peak LVP improved by 13 ± 1 mmHg with systolic assist, and the LVSW increased by 762 ± 68 mmHg*mL (+69%). The diastolic pressures showed a slightly different trend, with the overall DBP changing by only 1 ± 3 mmHg, and the pulmonary artery diastolic pressure (PADP) decreasing by 3 ± 3 mmHg. The mean pressures, MAP and PAMP, increased by 6 ± 1 mmHg and 2 ± 2 mmHg, respectively. Finally, regarding venous return pressures, the overall CVP decreased by 1 ± 1 mmHg, and the LVEDP remained unchanged (0 ± 1 mmHg).

2.4. Discussion

The EpicHeart™ Device is a non-blood contacting epicardial heart assist device that when activated, increases the stroke volume and offloads the heart. Additionally, this technology is low-profile and is implanted successfully via minimally invasive methods. In this study, the EpicHeart™ Device was implanted in five animals for further assessment of effects in an acute failure model. Esmolol was administered to decrease the force and rate of heart contractions, therefore reproducing the depressed blood pumping capacity seen in cases of heart failure or cardiogenic shock. Physiologic blood pressures and CO were recorded during periods of short-term device standby and device assist, and were averaged for individual animal study device performance as well as overall trend.

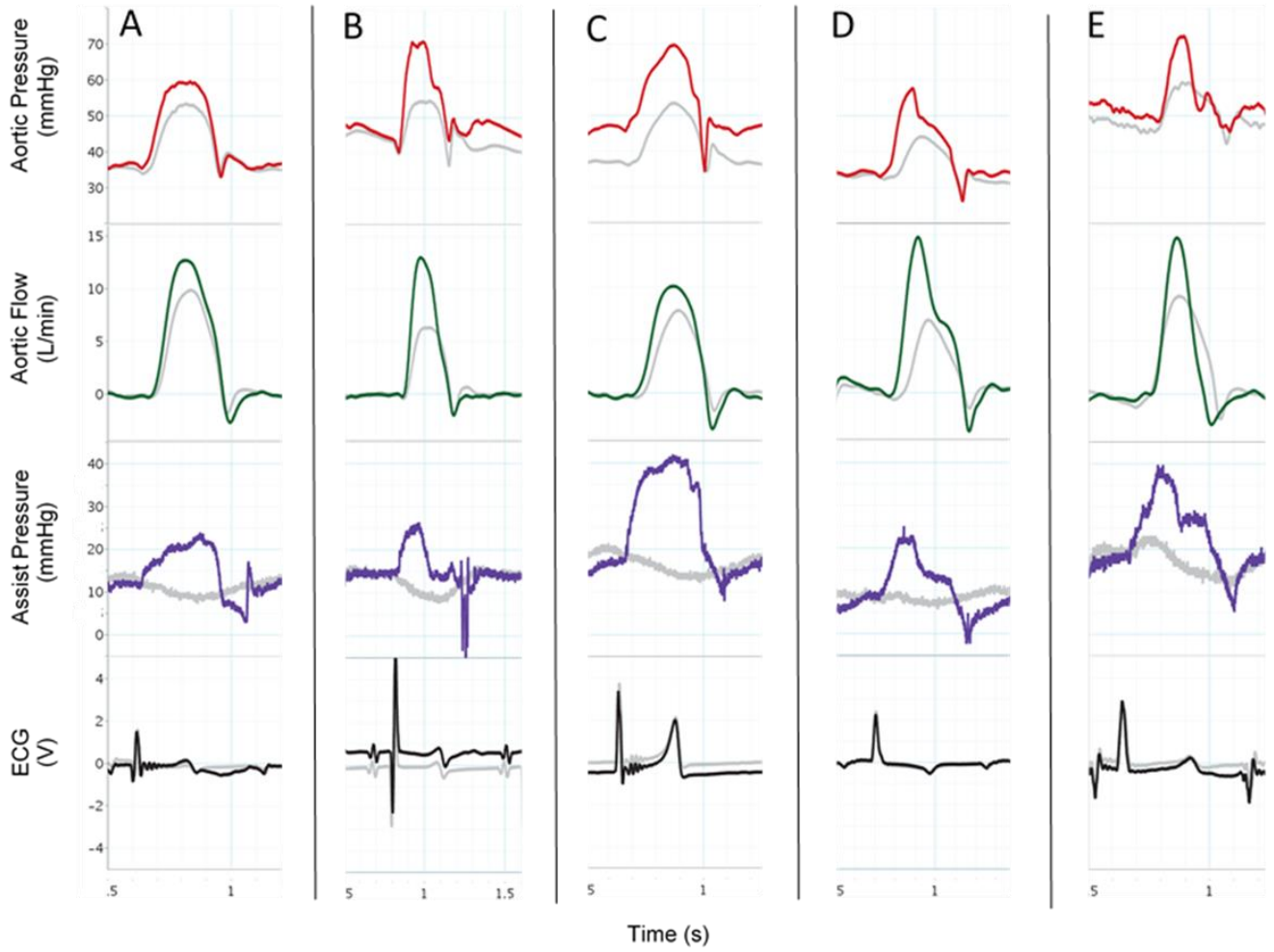

Figure 7. Hemodynamic waveforms sampled from each study; A, B, C, D, and E indicate Study 1, 2, 3, 4, and 5, respectively; the gray line shows the unassisted waveform, and the colored lines indicate the hemodynamic waveforms during assist

The repeated success of minimally invasive deployment on the first attempt shows significant confidence in the practical implantation of this device. Moreover, the device was implanted at two different study locations with different surgical teams, further demonstrating the ease of use of this technology. In the single case where minimally invasive deployment was not successful on the first attempt, the distal end of the EHI prototype was simply caught on the small pericardial access incision at the apex, preventing advancement from the deployment tube. The surgeon made a slight adjustment to the pericardial incision, allowing for a successful minimally invasive deployment on the following attempt. Given that many patients with heart failure are considered high-risk for major surgery, a minimally invasive device placement procedure is desirable. Additionally, the swift deployment time – as quick as 15 seconds after access to pericardial sac established– opens up opportunities for other applications of this technology, such as in cases of acute cardiogenic shock or cardiac arrest outside of the OR.

While the deployment process was without any major complications, there were two cases where an assessment of deployment on hemodynamics was more complicated. In the first study, dobutamine (a sympathomimetic drug that stimulates the β_1 receptors) was administered immediately upon deployment, effectively increasing the post-deployment hemodynamics (HR, BP, CO). Although periodic beta-agonist drug intervention for maintaining normal blood pressures is common in surgical procedures, drug intervention was avoided in successive animal studies in attempt to narrow the cause of any hemodynamic changes to those that are device-related. In studies 2, 3, and 4 the CO recovered by at least 83% after closing the chest. The final study was the only case

to show a further reduction in the CO at steady state. However, this animal was tachycardic, so procainamide was used to lower the HR; the pre-deployment HR was 120 BPM (CO 3.9 L/min), and reduced to 84 BPM with a CO of 2.6 L/min at steady state. For this reason, SV is a better indicator of changes in cardiac function with device placement. In previous work with this device, PV Loops were used to demonstrate that this device does not impede heart function.[10,11] In the present study, flow probes were used in place of a PV Loop catheter, and once again, there was no significant difference in LVSV between pre-device placement and steady state post-implant. Figure 8 shows representative aortic flow waveforms collected pre-deployment and at steady state post-deployment – notice that there is almost no change in aortic flow.

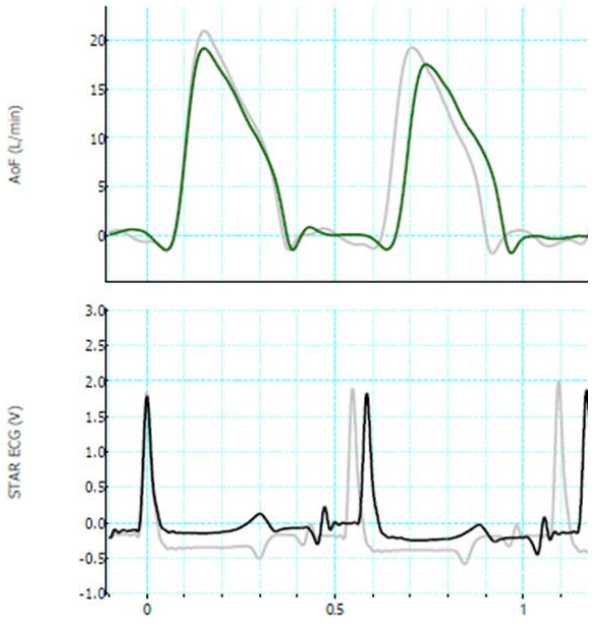

Figure 8. Aortic flow before (light gray) and after EHI placement; notice that there is almost no change in LV SV

In this study, device performance was considered separately for each animal due to variations in healthy baseline, as well as variations in how each animal responded to surgery and esmolol (Figure 6). Only the relative changes with device assist were considered in the overall averages, providing a clear assessment of the device (Table 2). Epicardial ventricular assist with this device recovered the baseline CO by at least 64%, with the highest at 100% recovered. It is interesting to note the correlation between CO recovery and baseline; animals with a lower baseline responded better to the assist, based on the trend of having a higher percent recovery. This potentially shows that the technology is more effective in patients with lower pumping capacity. In the device study by Roche et al, a recovery of ~97% of Baseline CO was reported with ventricular assist when failure state was ~2.7 L/min.[12] Here, if we only consider animals with a baseline of less than 3.0 L/min, the average recovery with EpicHeart™ assist is 97%. The trend in Figure 6 suggests that device performance is on the order of 0.7 L/min, and when the baseline is low then device assist can bring the animal back to baseline output (studies 2 & 5), whereas when the baseline is high then device assist does not return the animal to baseline (studies 1 & 4).

In addition to increasing LVSV, the device increased RVSV without impeding normal right-heart function. While epicardial ventricular assist resulted in parallel changes in SBP, the PAMP remained 1/3 of the MAP with assist. This indicates that uniform LV/RV epicardial compression did not over-assist the right heart, where lower pressures are the norm. Furthermore, there were no increases in LVEDP with assist, indicating no increases to LV preload due to elevated pulmonary pressures. Finally, the

reduced CVP and PADP both indicate that device assist offloads the heart and reduces the RV preload.

2.4.1. Study Limitations

The esmolol acute failure model, although commonly used for preclinical testing of similar devices, is not a true HF model. A high dose of a beta-blocker, such as esmolol, is very effective in reducing the cardiac contractile strength and stroke volume. However, beta-blockers do not result in the pathologic cardiac tissue growth and remodeling seen in many cases of heart failure. Additionally, esmolol causes dilation of the great vessels, resulting in significantly reduced pulse pressures. Therefore, the device needed to overcome significantly reduced pressures typically not seen in heart failure patients, which may have affected the recovery of cardiac output. A low preload may have limited the effects of epicardial ventricular assist, whereas a low afterload may have enhanced it. The next stage of evaluation of this technology will include testing in an ovine model of chronic HF with dilated LV, providing insight on these topics left unanswered by the esmolol acute failure model.

Another potential limitation is the PAP data excluded from 2 of the 5 studies. It was suspected that the distal end of the Swan-Ganz catheter may contribute to pre-ventricular contractions (PVC)s, in turn limiting device triggering and operation. Therefore, the transducer was retracted to no longer cross the PA valve, and consequently the frequency of PVCs was greatly reduced. While the PAP data from 3 studies provides solid information, continued efforts will be made to assess the pulmonary pressures by measuring the RVP in future studies.

The final potential limitation to the study design is the inclusion of only 5 animals. Nevertheless, numerous paired standby and ventricular assist samples were collected per study for higher confidence in results, as opposed to collecting only representative samples during previous proof-of-concept studies. To minimize bias, all samples where the device was properly triggered and activated, as well as met the failure state inclusion criteria, were included in the results reported from this study.

The only device-related limitation of significance was the limited availability of prototypes, and thus it was possible for the devices to not be the ideal size for particular hearts. Preliminary imaging was not completed prior to each study for device sizing; rather, a device was chosen from a set of up to 3 sizes, based on intraoperative fluoroscopic imaging and by recommendation of the lead surgeon. While the passive component of the EHI device has significant volume, and can be adjusted for variations in circumferential dimension, substantially larger hearts were more difficult to accommodate. This was apparent in study 2, where the heart was unexpectedly large in the axial dimension, and only one size of the EHI prototype was available; this animal experienced the most significant decrease in SV and increase in CVP immediately upon deployment. However, since the SV recovered to 85% of the pre-deployment level, and CVP remained within a physiologic range, the procedure was continued. An additional indicator of a potentially undersized device was the LVEDP. In study 2, the LVEDP increased slightly upon deployment, and instead of reducing upon chest closure, this LV filling pressure continued to rise. A similar situation occurred in study 4, which also reflected the changes in SV and CVP reported for deployment in study 2. In study 5, however, the LVEDP remained

unchanged with device placement, in combination with almost no change in SV, likely indicating an ideal fit. By study 5, additional sizes of the EHI prototype were available for the procedure. Future studies will incorporate a wider range of available device sizes.

2.5. Conclusion

Results of the current study show the efficacy of the EpicHeart™ Device to assist the failing heart acutely. Minimally invasive surgical implantation was a repeated success, combined with significant recovery of cardiac hemodynamics with device assist during acute failure. The next phase in developing this technology will include longer-term implantation, and a pilot investigation of the EpicHeart™ in a chronic heart failure model with dilated growth and remodeling.

3. SIMULATION OF EPICHEART™ EFFICACY

3.1. Introduction

There has been a growing need for simulation tools in research. By developing robust simulation methods, researchers can better plan for *in vivo* studies, ideally allowing for a reduction in the total number of subjects necessary for exploring the study aims. Additionally, simulation allows for better planning when transitioning from acute studies to chronic studies. In regards to investigating the preclinical efficacy of the EpicHeart™ Device, a direct cardiac compression (DCC) device with novel features that enable less invasive implantation and more physiological cardiac deformation, several unknowns will remain after the acute failure model studies have concluded. Specifically, it remains to be seen how a subject with normal to elevated hemodynamic pressures or a pathologically remodeled heart will respond to this DCC, as this morphology is absent in the acute models but is characteristic of many clinical cases of heart failure.

To this end, a modified Harvi iPad application with the capability to simulate EpicHeart™ function in a clinical model is in the early stages of development. This new application builds on the existing Harvi simulation tool – a real-time, interactive simulation of the cardiovascular system used for exploring basic hemodynamic principles in health and disease, and for predicting the effects of device- and surgical-based treatments for heart failure. The Harvi app has been used by other groups for clinical simulation, with examples that include patient selection for mechanical circulatory treatment,[16] prediction of the effects of an interatrial shunt for patients with elevated

PCWP,[17] and prediction of the hemodynamic effects of varying degrees of right ventricular support in patients with pulmonary arterial hypertension.[18]

Although the indication for the technology has yet to be specified, the benefit of such a simulation tool to DCC device design and development as well as future clinical use is substantial. The next step in the design process for this simulation tool is to verify the performance specifications. The simulation tool presently includes customizable EpicHeart™ inputs with simulated physiologic outputs. To this end, the present study reports the results of a pilot study of simulating device action compared with *in vivo* data of device action.

3.2. Materials and Methods

3.2.1. Device Assist Simulation Controls

The DCC device was simulated using the parameters listed in Table 3. All data simulated was during assist once every cardiac cycle, or a Ratio of 1:1. The Offset is the device pressure during diastole, and is intended to model any passive restraint on a dilated heart. Since the data modeled here is an acute heart failure model, this parameter was not evaluated in this study; the value was 0 mmHg for all simulations. The Delay is intended to model any time delay between the start of IVC and the start of inflation of the device. There was no delay in the selected data for this simulation study, and therefore the value for this input was 0 ms. The "Trigger to Assist Delay" feature in the Driver user interface is a time delay from the QRS trigger to the start of IVC. Since the model defaults to initiating assist with the start of IVC, there is no need for a delay in this simulation.

Table 3. List of Inputs for Device Simulation

INPUT	UNIT	DESCRIPTION
Ratio	BPM: n	Ratio of assist cycles to cardiac cycles
Offset	mmHg	Device pressure during diastole
Delay	ms	Time delay of inflation from start of LV contraction
Rise	mmHg/ms	Rate of pressure rise
Amplitude	mmHg	Pressure during full inflation
Decline	mmHg/ms	Rate of pressure decline
Duration	ms	Duration of pressure pulse

The current simulation design involves a trapezoidal pressurization waveform with a linear inflation rate, a stable peak pressure, and a linear deflation rate. The device assist pressure was collected using a Millar Mikro-Tip® Catheter Pressure Transducer (Model SPR-320, Size 2F) placed in a fluid chamber (the passive component) located between the active compressive assist component of the Implantable and the surface of the heart. This transducer was used to record the instantaneous pressure applied by the device to the outside of the heart.

The goal of this investigation was to simulate systolic assist; therefore, only the systolic components of the device pressure waveform were included in the average

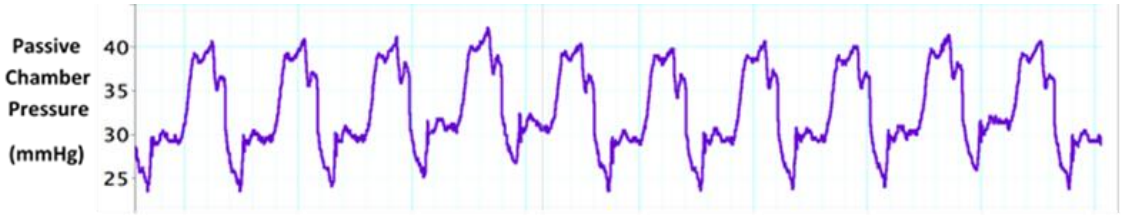

Figure 9. Instantaneous device assist pressure, measured by floating a Millar in the fluid of the passive chambers, providing a metric of epicardial assist

pressure calculations. Since passive pressure is not constant during assist (Figure 9), and fluctuates between inflate and deflate with systole and diastole, the Amplitude was approximated using an average weighted with systole:

$$\langle x(t) \rangle = \frac{\int_{t_i}^{t_f} \omega(t) * x(t) dt}{\int_{t_i}^{t_f} \omega(t) dt} \quad (1)$$

where $\omega(t)$ is the weight function. To create the weight function, we used the LVP, mean LVP (<LVP>), and the signum function:

$$\mathrm{sgn}(x) = \begin{cases} 0 \text{ if } x \leq 0 \\ 1 \text{ if } x > 0 \end{cases} \quad (2)$$

The first step was to subtract the mean LVP from the original LVP channel. Then, we calculated the signum (Eq. 2) of the resulting signal to get the weight function $\omega(t)$:

$$\omega(t) = \mathrm{sgn}(LVP - \langle LVP \rangle) \quad (3)$$

To find the systolic components of the assist pressure channel, we multiplied:

$$\omega(t) * p(t) \quad (4)$$

Then we applied Eq. 1 to find the average device pressure, <p(t)>, weighted with systole:

$$\langle p(t) \rangle = \frac{\int_{t_i}^{t_f} \omega(t) * p(t) dt}{\int_{t_i}^{t_f} \omega(t) dt} \quad (5)$$

This provided an assist pressure averaged over the systolic period, and excluded any diastolic components. To mitigate any potential inaccuracies in calibration of the transducer – due to temperature variation between room temperature and body temperature – the relative pressure was calculated by taking the systolic weighted average pressure during assist, and subtracting off the systolic weighted average pressure during the preceding sample of standby data.

The Rise and Decline of assist were determined based on the average slopes of the device pressure signal. These were determined using LabChart software, by taking the instantaneous derivative of the device pressure signal and multiplying by the systolic weight function (Eq. 3) to create two new signals, one with only positive instantaneous derivatives, and one with only negative instantaneous derivatives:

$$\text{Rise} = \omega(t) * \left[\frac{\frac{dp(t)}{dt} + \left| \frac{dp(t)}{dt} \right|}{2} \right] \quad (6)$$

$$\text{Decline} = \omega(t) * \left[\frac{\frac{dp(t)}{dt} - \left| \frac{dp(t)}{dt} \right|}{2} \right] \quad (7)$$

The instantaneous slopes are plotted with the passive pressure, p(t), in Figure 10. The cyclic maxima and minima of these positive and negative slopes were averaged to determine the Rise and Decline rates of pressure (inflation and deflation rates). The result was a slope in mmHg/s, which was rounded to the nearest 0.2 mmHg/ms to accommodate the model units.

Finally, the Duration of assist was simulated using the average time duration of each systolic weight function cycle:

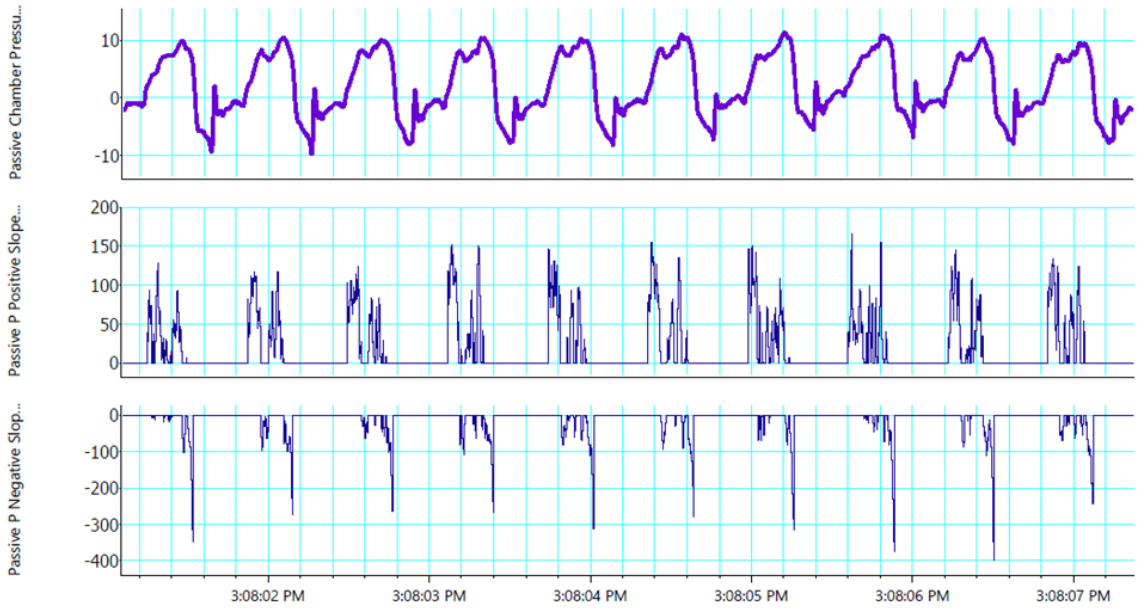

Figure 10. LabChart channels displaying the passive pressure, p(t), and the instantaneous derivatives for positive and negative slopes

$$\text{Duration} = \frac{\int_{t_i}^{t_f} \omega(t)\,dt}{n} \qquad (8)$$

Where n is the number of cardiac cycles in the data sampled from t_i to t_f. Figure 11 shows the simulated assist pressure plotted with the *in vivo* assist pressure.

3.2.2. In vivo Data Source

All hemodynamic pressures were recorded using either a Millar solid-state pressure transducer or a fluid-filled catheter. The CO from all studies was acquired using a Transonic COnfidence flow probe, placed on the ascending aorta. The source of hemodynamic data is described in Section 4.2. One key difference was where this study cited a sample inclusion criteria based on the CO relative to pre-failure baseline, all

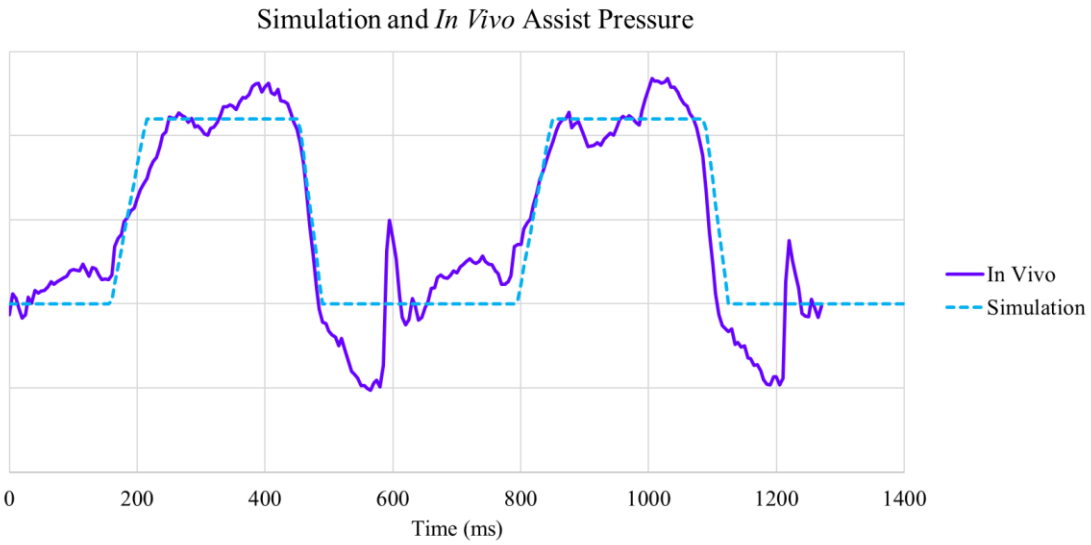

Figure 11. Assist pressure waveforms, comparison of *in vivo* to simulation

samples were included in this simulation study to maximize the sample population for the best possible assessment of model performance.

One parameter that was not measured in these *in vivo* studies was the PCWP. However, as this parameter is often used as an approximation of the LV EDP, which was measured using a solid-state pressure transducer (Millar) placed in the LV, the LV EDP data was used to approximate the PCWP. Additionally, there were two studies where PAP was missing; during these studies, it was suspected that the source of recurrent pre-ventricular contractions (PVCs) was the Swan-Ganz transducer for PAP, and thus the catheter was retracted to no longer cross the PA valve. Therefore, the PAP inputs were approximated for these two studies, using the LV EDP as the PA diastolic pressure, and

applying a 10 mmHg PA pulse pressure. This was based on the average PA pulse pressure during acute heart failure in the two studies where the PAP was measured *in vivo*.

Cardiac chamber volume and ventricular wall thickness were approximated based on a sample of CT dimensions acquired during a previous scan of an anesthetized ovine. As this was an acute HF study with no pathologic growth and remodeling, the cardiac geometry was held constant for all simulations. Additionally, data analysis focused on the relative change in hemodynamic parameters, and thus results were expected to be minimally impacted by not using exact cardiac geometries. In place of using the cardiac volumes from the CT to calculate EF, this parameter was calculated for the simulation using the SV – defined by CO/HR – from each sample, and only the LV EDV from the CT. On a similar topic, the LVSW was not calculated using volume data. SW is most commonly found as the area within a PV Loop, however since ventricular volume was not measured *in vivo*, an alternate method was applied. Knowing that power, P(t), in a fluid system can be found using the following equation:

$$P(t) = p(t)*Q(t) \quad (9)$$

Left-heart power could be calculated using the LVP and Ao flow. This data was then converted from mmHg*mL/s to Watts for assessment of the simulated LV CPO.

Finally, knowing that work is the integral of power, we found LVSW by taking the integral of the instantaneous power channel, and dividing by the number of cycles n in the sample from t_i to t_f:

$$LVSW = \frac{\int_{t_i}^{t_f} P(t)dt}{n} \quad (10)$$

3.2.3. Evaluation of the Simulation

The *in vivo* hemodynamic data during device standby provided the inputs for the "Patient Simulator" feature of the application to establish the simulated patient baseline (summarized in Table A 1). Then, the "CorInnova Device" feature was turned on, using the process described above to determine the inputs (summarized in Table 3). The steady state hemodynamic outputs under the simulated assist conditions were compared to the *in vivo* hemodynamic data during assist conditions. Only certain hemodynamic outputs were included in this pilot investigation, based on the availability of *in vivo* data for verification (summarized in Table A 2). To normalize the data, the relative change in each parameter from Standby to Assist – denoted as the Delta value – was compared between simulation and *in vivo*.

$$\Delta = \text{Assist} - \text{Standby} \quad (11)$$

The Delta values were averaged for each animal study, to reveal any differing results due to study conditions. Standard deviations reflect variation in data between paired samples for the same study. Finally, due to differing sample sizes per animal study, these mean Delta values from each animal were averaged together (n=4) to provide an overall assessment of simulation accuracy, weighted equally for each animal study. Standard deviations here reflect variation in overall performance between each animal study.

As a metric to compare the simulation to the *in vivo* data, we calculated an expectation percent, defined as:

$$\%\ \text{expectation} = \frac{\Delta\ in\ vivo}{\Delta\ \text{simulation}} \quad (12)$$

The simulation was chosen as the expectation, as the model assumes no energy lost between epicardial compression and ventricular assistance, and thus will simulate Delta values as anticipated. A metric above 100% would indicate that the device performed above expectations, where below 100% would indicate that the device provided cardiac assistance to the patient below expectations. This was a blinded study, where the simulation operator was provided with only the hemodynamic data during *in vivo* device standby, and the proper device settings for that paired sample, and an analyst compared the results of simulated device assist to the hemodynamic data during *in vivo* device assist.

3.3. Results

3.3.1. Individual Study Simulation Performance

The results of the delta values for each hemodynamic parameter are summarized in Table 4 for comparison between simulation and *in vivo*, as well as Figure 12 and Figure 13. See Figure A 1 and Figure A 2 for hemodynamic waveform comparison between *in vivo* and *in silico*. Individual study analysis revealed Study 2 to be an outlier. The changes in systemic pressures (SBP, DBP, MAP) as well as pump function (SV, CO, LVSW, LVCPO) with device assist were consistently lower *in vivo* than the simulated hemodynamic outcomes. In contrast, these parameters showed paralleled results in the simulation and *in vivo* for the remaining three studies.

The change in LVEDP predicted by the simulation was mostly opposite to the trend *in vivo*; where the model predicted an increase in LVEDP with device assist, the

results *in vivo* were generally unchanged. Similarly, the model consistently predicted an increase in DBP and PADP, where these parameters mostly decreased with assist *in vivo*.

Finally, there was a correlation between EHDP and SBP, especially in Study 1 and Study 4 where the increase in SBP was equivalent to the EHDP.

3.3.2. Overall Simulation Performance

After assessing the model for each individual animal study, the hemodynamic parameters of interest were averaged over the four *in vivo* sample sets, to compare *in vivo* to in silico overall. Beginning with the systemic changes, the *in vivo* SBP and MAP values increased by 11 ± 1 and 7 ± 1 mmHg with assist, compared to 12 ± 4 and 9 ± 4 mmHg predicted by the model. In contrast, the *in vivo* DBP showed a trend opposite to that of the simulation; the simulation predicted an average increase in DBP of 7 ± 3 mmHg, when the average change in DBP was actually a decrease of 1 ± 3 mmHg. Finally, both the *in vivo* CVP and the predicted CVP showed a slight decrease in pressure with device assist; the model predicted an overall decrease in CVP of 2 ± 1 mmHg, while the overall effect *in vivo* was a decrease of 1 ± 2 mmHg.

The changes in pulmonary pressures showed a similar trend as the aortic blood pressures; the *in vivo* mean PAP increased by only 4 ± 4 mmHg with assist compared to 7 ± 3 mmHg in silico, and the systolic PAP increased by 8 ± 7 mmHg *in vivo* compared to 7 ± 3 mmHg in silico. Moreover, the diastolic PAP decreased by 5 ± 6 mmHg *in vivo* but increased by 6 ± 3 mmHg in silico; the trend in diastolic PAP was consistent with the trend in Aortic DBP. Finally, there was no change in LV EDP *in vivo* (0 ± 1 mmHg), however the model predicted a 5 ± 3 mmHg increase in LV EDP with assist.

Table 4. Summary of changes in hemodynamic outputs, comparison of simulation and *in vivo*

	STUDY 1 Δ		**STUDY 2 Δ**		**STUDY 3 Δ**		**STUDY 4 Δ**	
	Simulation	***In Vivo***	Simulation	***In Vivo***	Simulation	***In Vivo***	Simulation	***In Vivo***
SBP (mmHg)	11	**11**	18	**12**	8	**12**	10	**9**
DBP (mmHg)	6	**3**	11	**-3**	4	**0**	7	**-2**
MAP (mmHg)	8	**7**	15	**9**	6	**7**	8	**6**
PASP (mmHg)	7	**3**	12	**13**	5	**N/A**	5	**N/A**
PADP (mmHg)	5	**-1**	10	**-9**	2	**N/A**	5	**N/A**
PAMP (mmHg)	6	**1**	11	**6**	4	**N/A**	5	**N/A**
CVP (mmHg)	-2	**0**	-4	**-3**	-1	**-1**	-2	**1**
LV EDP (mmHg)	5	**0**	9	**1**	2	**0**	4	**-1**
LV SV (mL)	11	**9**	14	**5**	11	**14**	6	**4**
CO (L/min)	1	**0.9**	1.3	**0.5**	0.9	**1.2**	0.5	**0.4**
LV SW (mmHg*mL)	492	**828**	764	**683**	535	**764**	415	**580**
LV CPO (Watts)	0.13	**0.17**	0.23	**0.14**	0.11	**0.14**	0.12	**0.12**
EHDP (mmHg)	11	**11**	19	**19**	9	**9**	9	**9**

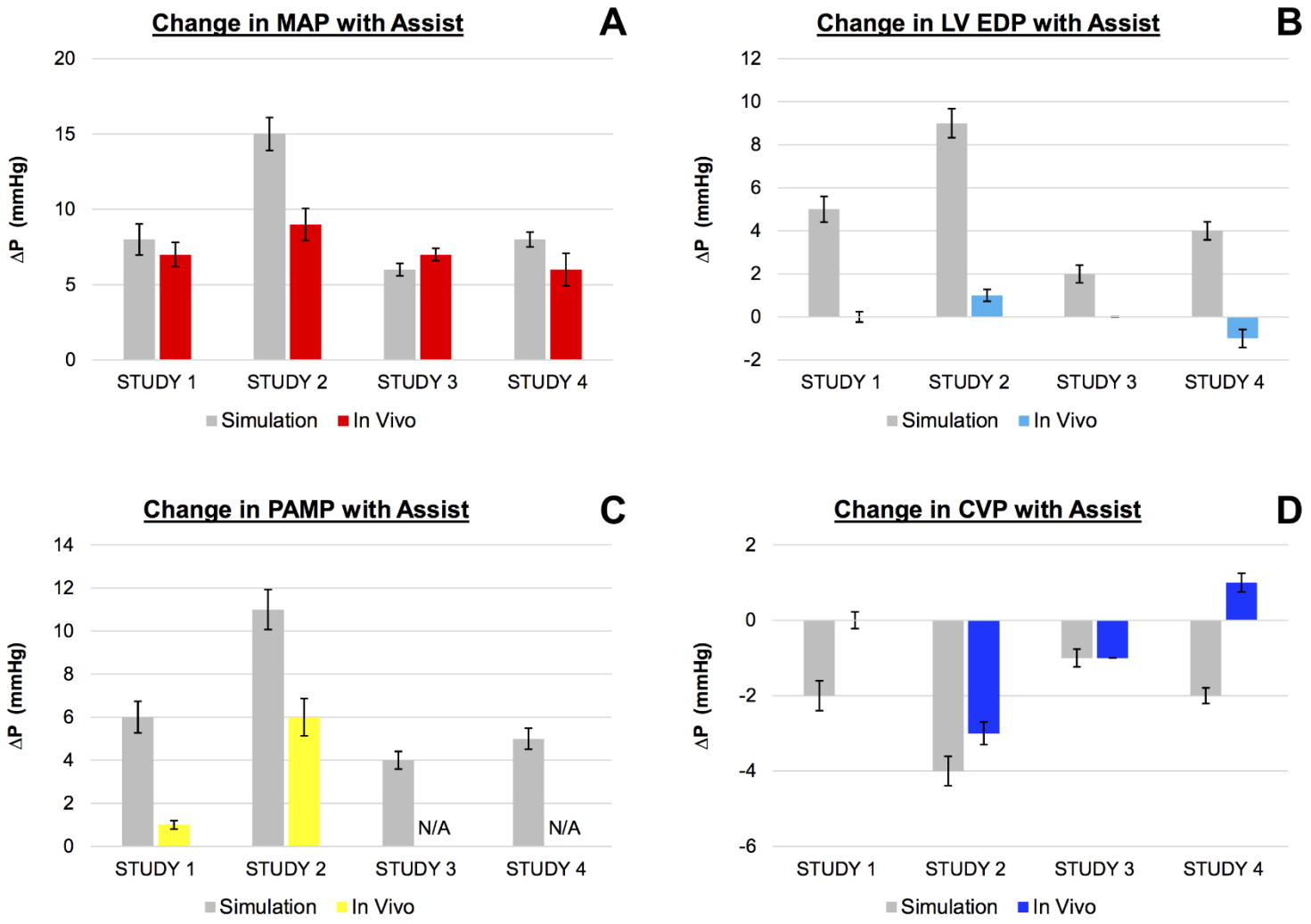

Figure 12. Changes in MAP (A), LV EDP (B), PAMP (C), and CVP (D) with device assist, *in vivo* and simulated

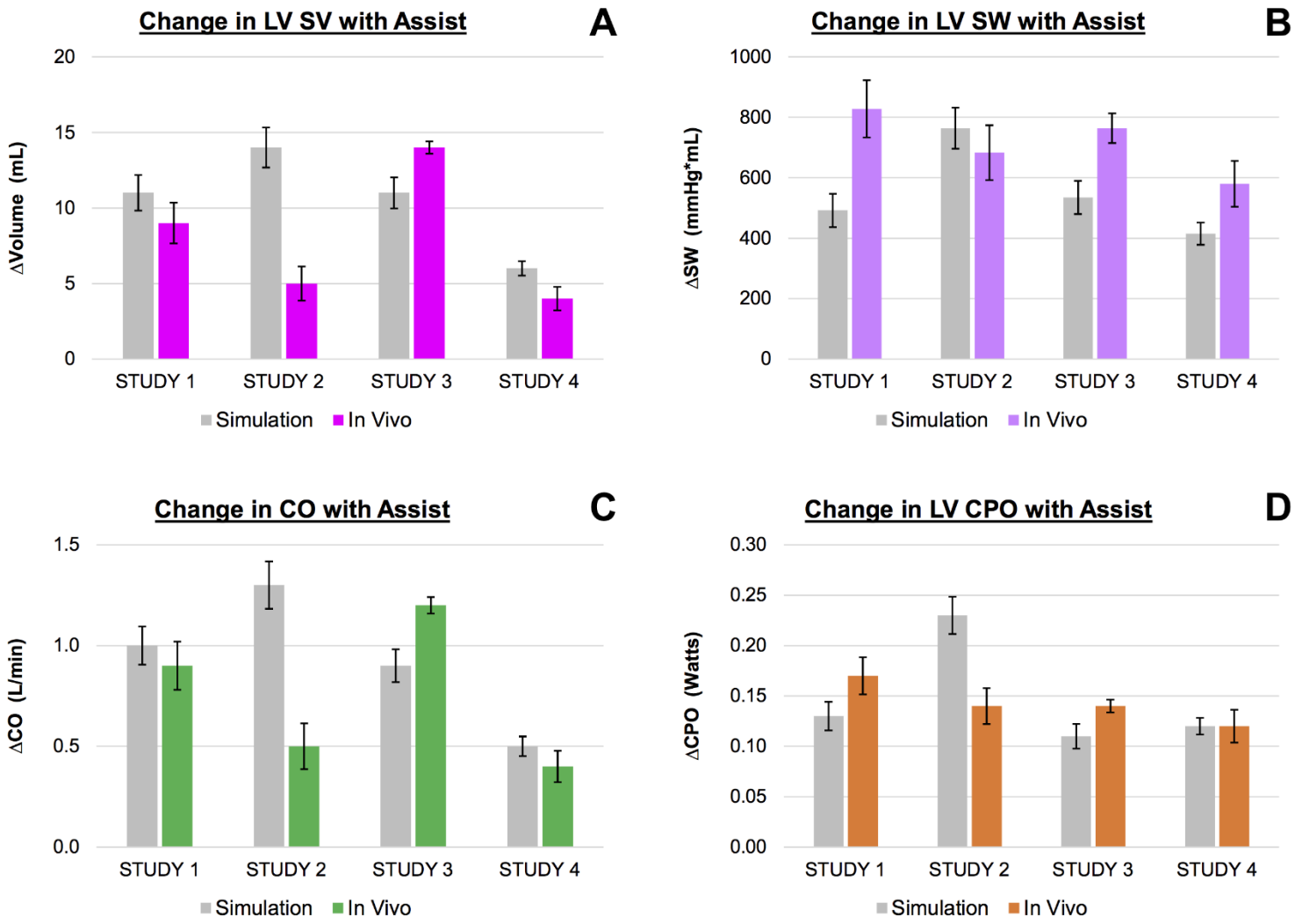

Figure 13. Changes in LVSV (A), LVSW (B), CO (C), and LVCPO (D) with device assist, *in vivo* and simulated

When evaluating the pump function of the heart *in vivo*, the LV SV and LV CO were 73% and 89% of the expected change in output. The LV CO increased by 0.8 ± 0.4 L/min with assist *in vivo*, and increased by 0.9 ± 0.3 L/min *in silico*. The LV SV increased by 8 ± 5 mL *in vivo*, and increased by 11 ± 3 mL in silico. Additionally, the LV SW was 129% of the expected results. This was the only cardiac pump function metric to exceed the expectations of the simulation (when considering model performance over all animal studies). Finally, the LV CPO was 93% of the simulated results, with an increase *in vivo* of 0.14 ± 0.02 Watts compared to an increase of 0.15 ± 0.06 Watts *in silico*.

3.4. Discussion

This study was a pilot investigation of a new application of the Harvi cardiovascular simulation program. This version of the Harvi platform builds on the existing iPad program, developed using the Burkhoff model of the cardiovascular system, with the added feature of the ability to simulate the effects of the EpicHeart™ Device. In developing this technology, the performance specifications needed to be verified. Thus, *in vivo* data from 4 acute ovine studies was used to simulate device standby conditions as well as assist conditions. The resulting effects on the cardiovascular system *in silico* and *in vivo* were compared by evaluating the absolute changes, as well as considering the model results as the expected outcome and the *in vivo* results as a percent of that expectation for certain parameters.

Perhaps the most unexpected result of this study was the change in LV EDP. The simulation data for each parameter defined the expected outcome. However, the LV EDP

was the only parameter to predict a trend with assist that was not anticipated by our group; the simulation resulted in an average increase in LV EDP of 5 ± 3 mmHg – in direct contrast to the anticipated decrease in LV EDP. It has been shown that mechanical heart assist will offload the heart, resulting in a decreased preload to the LV. This is usually observed by a measured reduction in LV EDP (effectively LAP). When the device was tested *in vivo*, there was 0 ± 1 mmHg change in mean LV EDP with assist. An average of no change with a standard deviation of 1 mmHg does not reveal a clear trend *in vivo*. However, the *in vivo* data was from acute studies, where cardiac decompression was not anticipated with short-term assist.

One potential explanation for the simulated increase in LV EDP is that it is a previously unknown consequence of biventricular assist with this device. During device operation, the goal is to maximize the epicardial systolic assist pressure. Although the ideal assist pressure is currently not defined, the Driver operator maintains the assist pressure within a reasonable range – typically below 30 mmHg. While maximizing the assist pressure reflects positive results in the increased output of the heart, it is possible that maximized assist pressures could have an adverse effect on the right-sided pressures. Specifically, it is possible that if the PAP was too high as a result of uniform RV/LV assist, the downstream LA pressures and LV EDP would be increased as well. If the pulmonary pressures are abnormally high, the likely *in vivo* or clinical outcome would be pulmonary edema. However, it is expected that auto-regulatory mechanisms will be stimulated by the biventricular assist, which should balance the increased pulmonary pressures.

Another possible explanation for the differing effect on LV EDP is that the model needs a proportional distribution of the effects of epicardial assist between the left and right side of the heart. The simulation predicted a decrease in CVP with a significant increase in LVEDP, where the *in vivo* results show a slight decrease in CVP, and almost no change in LVEDP. Additionally, the ratio of EHDP (EpicHeart Device Pressure) to LV ESPVR shift in slope appears to be 1:1 *in vivo* and in the simulation; however, the data from Study 1 – chosen for optimal device fit and presence of *in vivo* PAP data – reveals a smaller shift in the RV ESPVR with assist than predicted by the simulation. Given the differing RV ESPVR shift *in silico* compared to *in vivo*, combined with the significant predicted increase in LVEDP, it is possible that the model overestimates the effect on the right side of the heart. Further studies are needed to explore this theory.

3.4.1. Pump Function Expectations

The LV CO, LV SW, and LV CPO all increased *in vivo* with device assist, reflecting the anticipated changes in cardiac pump function. While the overall change in LV SV was only 73% of the expected outcome, the overall average LV SW exceeded expectations at 129%. This can be explained by the difference in method for calculating LV Power and LV SW.

The integral method overestimates the loop area because it includes the area under the EDPVR curve. Moreover, since the model predicted an increase in LVEDP, the EDPVR curve was shifted upward, further removing the *in vivo* LVSW from the predicted LVSW. While our method is a calculation of true work in a fluid system, and was used due to the absence of a volume transducer, it is not consistent with the model method.

Thus, efforts should be made to use a PV Loop transducer in future studies, permitting calculations of SW to be consistent with the clinical method of the area inside a PV Loop plot.

3.4.2. Simulation Outliers

The results of the individual animal studies suggest that Study 2 is an outlier. The predicted hemodynamic effects of device assist in this study were the most removed from the *in vivo* effects, compared to the other three studies. During this particular animal study, it was determined by observation of the lead surgeon and confirmed by fluoroscopic imaging that the EpicHeart™ prototype implanted was significantly undersized for the heart. This particular heart geometry was unusually long in the axial dimension; thus, the prototype was determined to be too small in the axial dimension. Figure 14 demonstrates the difference between an optimally sized device, and the fit observed in Study 2. Even with a relatively high EHDP, the increase in CO was only 38% of the expected change, as determined by the model (Figure 13). Additionally, it is interesting to note that the increase in transmural pressure no longer reflects the device pressure when the device is too short (as determined by the ΔSBP); the average EDHP in Study 2 was 19 mmHg, however the ΔSBP was only 12 mmHg. Other studies show at least a 1:1 relationship between the EDHP and the ΔSBP. The outlier results of this study due to a poorly sized device provide insight for the design of DCC devices, and have clinical implications for the effect of implanting an incorrectly sized DCC device.

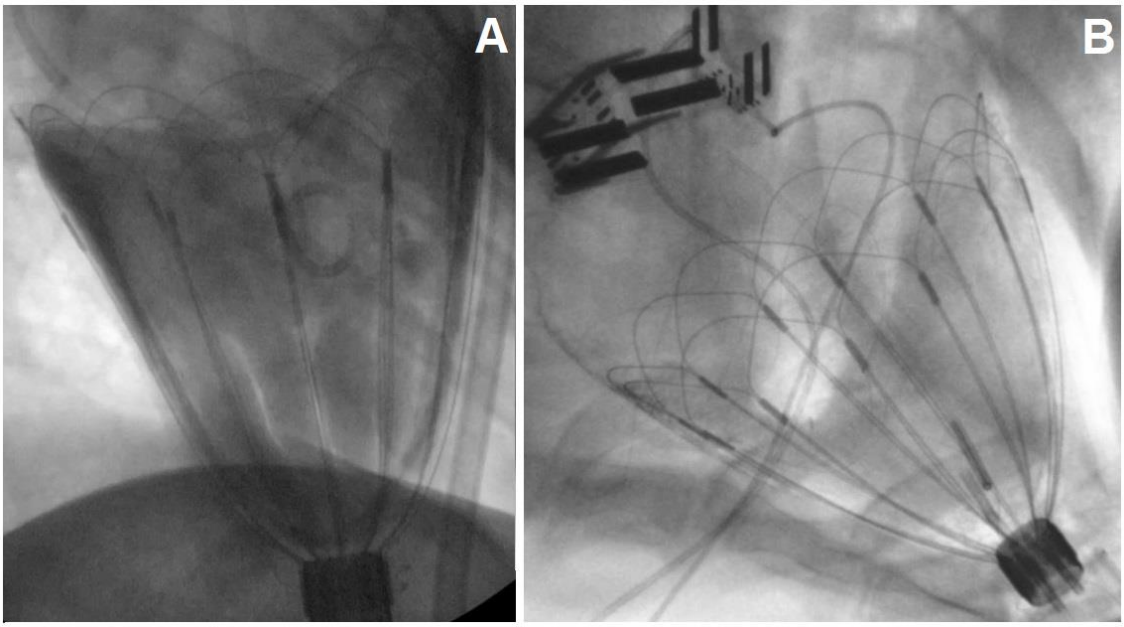

Figure 14. Fluoroscopic image comparison of Study 2 (A) and Study 5 (B); notice the abnormal geometry of the heart in A compared to B

3.4.3. Study Limitations

Certain limitations in this study have already been discussed, namely the deviations from the clinical/model method for calculating the SV, SW, and CPO. One other potential limiting factor here was the estimation method for PAP when that parameter was not measured *in vivo*. The Swan-Ganz catheter used to measure the PAP was retracted from the PA during certain animal trials, as it was suspected to be the cause of recurrent arrhythmias. Thus, the systolic and diastolic PA pressures were estimated based on the LV EDP and an average PA pulse pressure during failure of 10 mmHg. It is possible that the pulse pressure was underestimated, and in turn underestimating the systolic PAP used for simulation. Thus, this could potentially be the source of the *in vivo* results exceeding the expectations of the model for this parameter.

Additionally, we acknowledge that certain parameters measured *in vivo* were beyond the practical limitations of the Patient Simulator feature in the model. Specifically, the lower limit for the PADP input was 10 mmHg, however certain samples of *in vivo* data were actually lower than 10 mmHg, and thus these samples were approximated to 10 mmHg. Similarly, the lower limit for the Rise input of device simulation was 0.2 mmHg/ms, however in some *in vivo* samples, the Rise was as low as 0.1 mmHg/ms.

Next, there was a variation in the number of samples from each *in vivo* study – least at n = 3, to most at n = 36. Delta values were used to normalize any variation in baseline between animals, and all Deltas for each parameter were averaged over the sample set for each animal study. Then the individual study averages were subsequently averaged overall in order to provide equal weight for each study. Thus, any inexactitudes due to limited samples from an individual animal should be inconsequential.

An additional limitation was the method for simulating device assist. The epicardial systolic assist pressure waveform is modeled as a trapezoid with a linear pressurization, a constant peak pressure, and a linear depressurization. While this is a reasonable approximation for the pressurization waveform of the normal LVP, the device systolic assist pressure has some variation *in vivo*, partially due to each animal's unique response to the device. Moreover, the majority of this variation is likely due to exploration of the optimal assist pressurization during each proof-of-concept study and further development of the driver. However, as the model predicts the optimal results, this information reveals that an epicardial assist pressurization that more closely resembles the

trapezoid shape is perhaps desirable, and might be considered as a design specification to target when optimizing the driver.

While initially focusing on hemodynamic data was a valid starting point for simulation verification, we acknowledge that certain Harvi parameters were excluded from assessment in this study. Most notably, the cardiac geometry data – volume, ejection fraction, and wall thickness – was not verified in this analysis. Accurate cardiac geometry measurements from high-quality imaging (CT or MR) were beyond the scope of these acute failure studies. While a single ovine CT scan was available for use in estimating the baseline ventricular volumes and wall thicknesses, this information was not used to verify the volume simulation parameters. However, it is unlikely that this information was detrimental to the validity of the results of this study, as minimal change in cardiac volume is expected with the esmolol acute failure model since these are animals with no cardiac remodeling. Additionally, the baseline volumes were held constant for all simulations, normalizing any effect on hemodynamic performance specification assessment due to cardiac geometry. Finally, the MVO2 hemodynamic output was excluded from verification due to the absence of this data from all acute animal studies. It is currently unknown how the device under investigation in this study affects this parameter when implanted and activated.

3.5. Conclusion

This study described the results of a pilot simulation study of the EpicHeart™ Device – a DCC device with novel features that enable less invasive implantation and

more physiological cardiac deformation with systolic assist. Overall, the results of the comparison between *in vivo* and in silico were quite similar, indicating the technical specifications of the model require limited modifications for simulating this DCC device in an acute heart failure model. Future studies will include additional acute HF model verification, along with chronic HF model verification using echo data for assessment of the cardiac geometry parameters.

4. DEVELOPMENT OF A PNEUMATIC DRIVER FOR DCC DEVICES TO MIMIC INNATE CARDIAC VENTRICULAR PRESSURIZATION AND HEMODYNAMICS

4.1. Introduction

As significant effort has been devoted to optimization of the EpicHeart™ Implantable (EHI), a fully-developed pneumatic driver system is likewise important to optimum heart assist. Currently, it is unclear what driver pressurization (i.e. timing and magnitude of pressure applied) will result in the greatest increase in stroke volume; limited data on this subject has resulted from preliminary studies. In addition to the likelihood of suboptimal hemodynamics, inappropriate timing of pressurization may be detrimental to healthy cardiac tissue. Specifically, if the pressurization rate, duration, or timing of onset is too late in systole, the EHI may still be pressurized during isovolumetric relaxation (IVR), in which case the device may restrict rapid filling in early diastole. In contrast, if the EHI is pressurized prematurely, transmural pressure may be applied prior to papillary contraction – resulting in possible regurgitation through the AV valves due to compromised valve coaptation or interruption of atrial systole. Over an extended period of time, this improper timing of transmural assist may lead to papillary tissue damage. Clearly, pressurization onset time, rate, duration, and waveform morphology are vital to heart assist, and will be further explored in this study.

4.2. Methods

Three unique versions of the EpicHeart™ Driver were investigated in this study. A description of the control parameters and components of each version is detailed in the following sections.

4.2.1. Parameters to Adjust for Heart Synchrony

While the electrical-pneumatic delay in the Driver is minimal (~15ms, see Figure 15), there is a native electrical-mechanical delay in the normal heart. Therefore, one of the parameters used for synchronization between Driver function and heart function was the Trigger to Assist Delay (TAD). Figure 16 explains the basis of this parameter, demonstrating the time between ECG Trigger and the end of atrial systole. As the physiologic electrical-mechanical delay varies between subjects and contractile state, this parameter was a manual user input to be adjusted as needed during *in vivo* testing. The measured time between the ECG Trigger (coinciding with the peak of the R wave) and the start of cardiac isovolumetric contraction (IVC) during device standby quantified the minimum value for TAD. Proper synchronization with heart function was verified by overlaying the device passive pressure waveform and the left ventricular pressure waveform to visually check for synchronization between EHI pressurization and IVC.

After defining the timing of optimal initiation of assist, the user determined the Inflate Duration (ID). This user-defined time parameter specified how long the Inflate solenoid valve was open to the Driveline, and thus the EHI (see Figure 17 for the Inflate valve). Together, the TAD and ID determined the Assist Duration (AD), defined as the time from the ECG Trigger to Inflate valve closure. The AD was adjusted within the limits

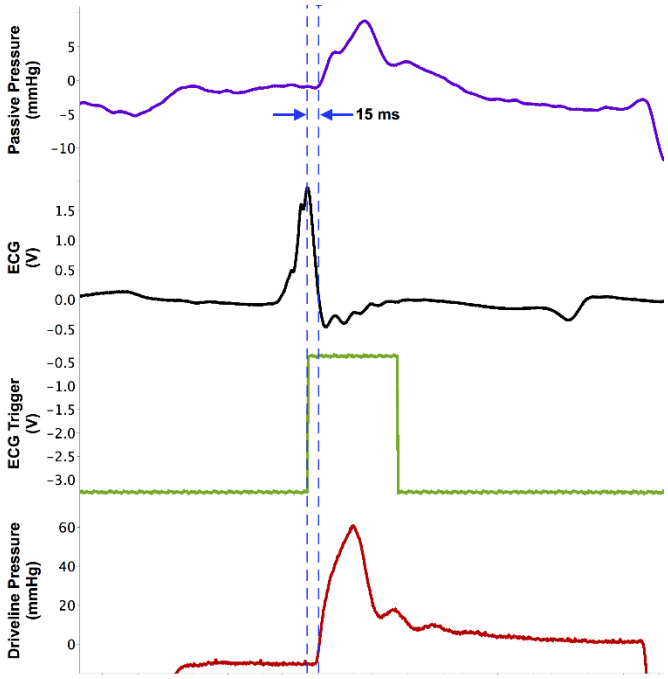

Figure 15. Waveform demonstration of the electro-pneumatic delay in the driver; notice the QRS peak and the ECG trigger are almost coincident, with only a 15ms delay from ECG trigger to the start of passive chamber pressurization

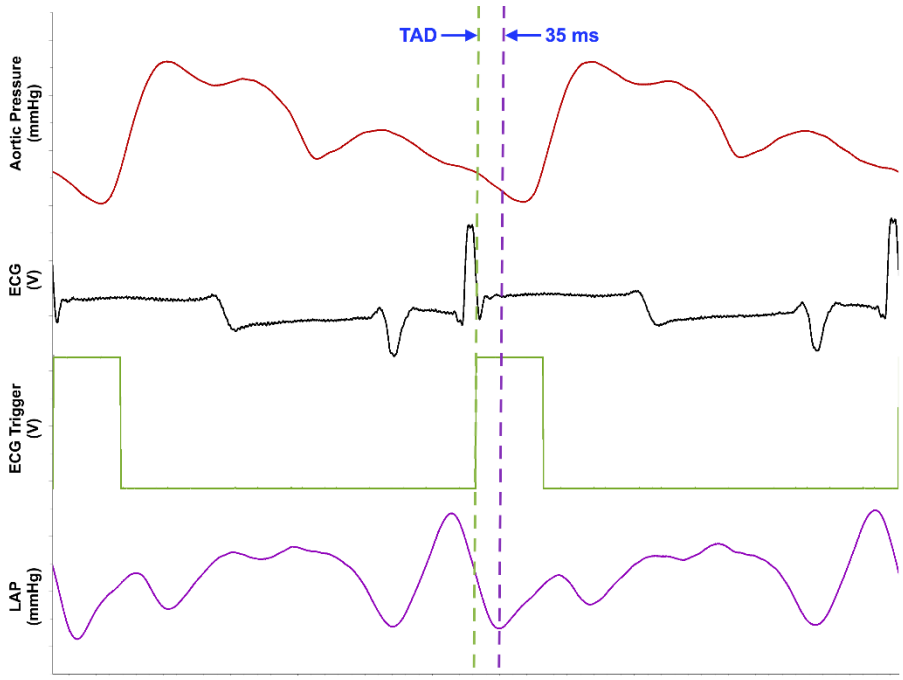

Figure 16. Waveform demonstration of the need for a Trigger to Assist Delay (TAD); notice the significant delay of 35ms from the trigger to the end of atrial systole

of the software, and in a method such that the maximum increase in cardiac SV was achieved without compromising the EHI chamber integrity.

Finally, in connection with the timing of solenoid valve activation, it was possible to modify the rate of pressurization of the EHI. The rate of pressurization was adjusted such that the maximum stroke volume could be achieved. It was unknown if a rapid pressurization rate or a slower rate would yield the greatest stroke volume, hence both conditions were explored. The pressurization rate was modified by adjusting the reservoir pressure, and/or by modifying the pneumatic driveline (i.e. pneumatic capacitor).

4.2.2. Driver V1: Parallel Pneumatic Disks, Regular Driveline

This generation of the driver includes updated hardware featuring additional solenoid valves as well as pneumatic isolator disks (safety disks) which mechanically isolate the EHI from the pressure reservoir. This limits the amount of volume available for infusion into the EHI for each inflate cycle, and the EHI is vented to atmosphere following each inflation cycle. This method of volume delivery limits the available pneumatic stroke volume, while providing a safety mechanism which mitigates the potential for device over-inflation. Additionally, each solenoid valve is individually controlled with unique valve states for highly customizable assist. The pneumatic hardware for the Parallel Driver is summarized schematically in Figure 17.

4.2.3. Driver V2: Parallel Pneumatic Disks, Pneumatic Capacitor Driveline

This version of the Driver has the same hardware setup as V1, however includes a pneumatic capacitor in line with the driveline to attenuate the pressurization spike seen within the chambers of the EHI with a regular driveline, while extending the pulse width

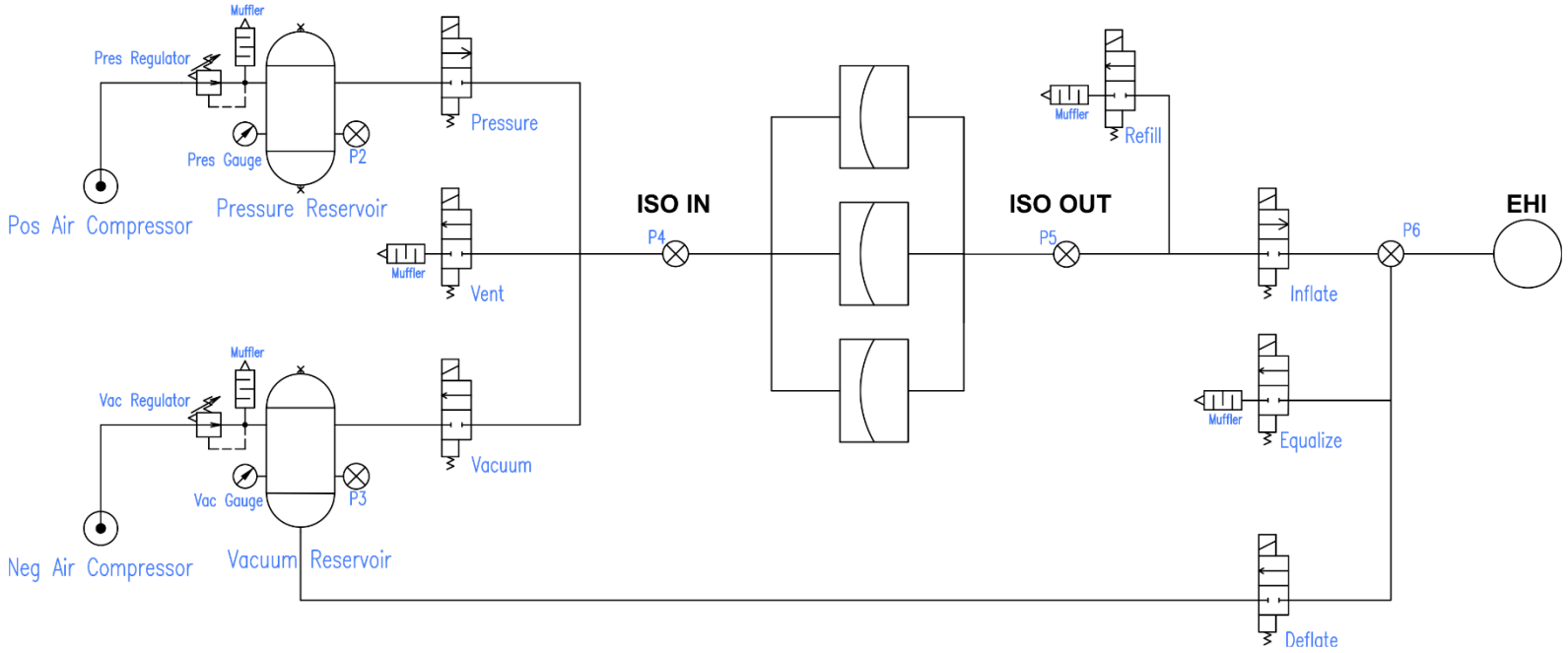

Figure 17. Pneumatic hardware schematic of the Parallel Disk driver; P1-6 are pressure transducers; each solenoid valve is labeled by name, Pressure, Vent, Vacuum, Refill, Inflate, Equalize, and Deflate; the ISO IN and ISO OUT label the input and output side of the pneumatic isolators; EHI labels the output of the driveline to the EpicHeart™ Implantable

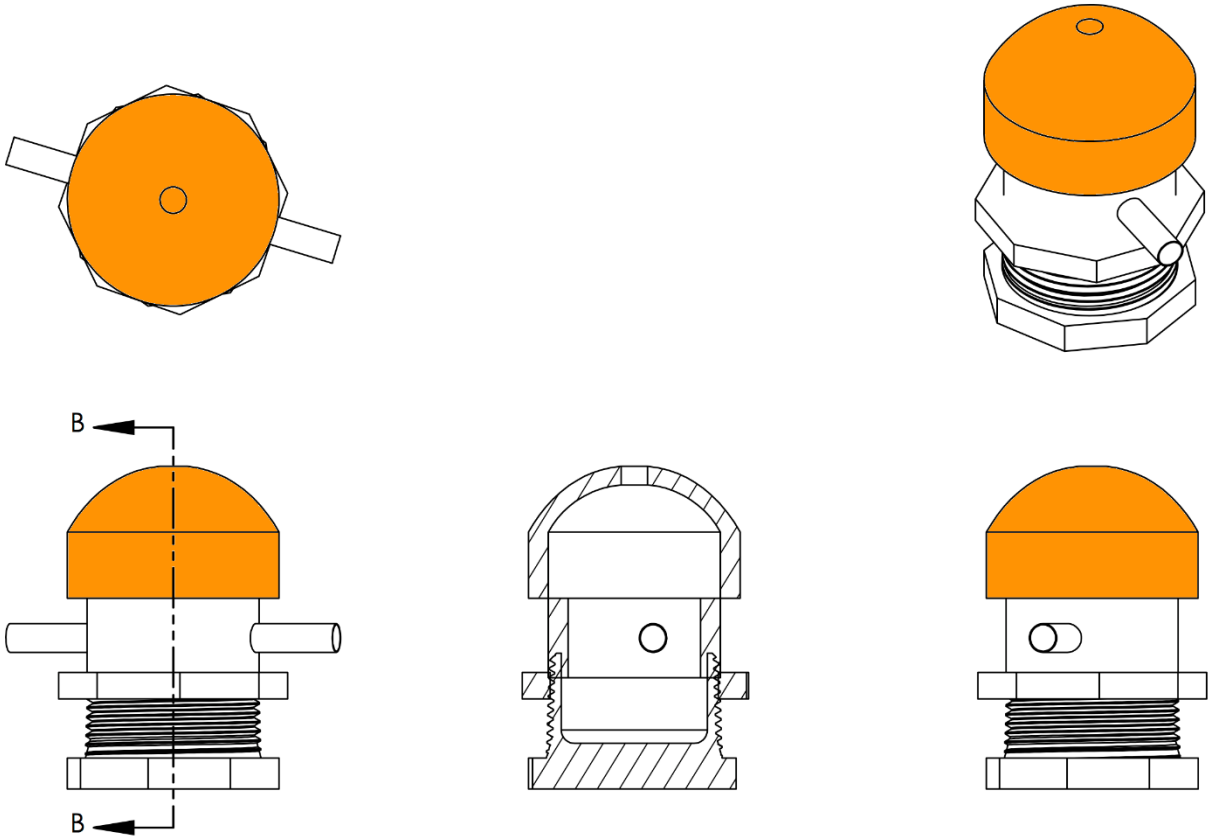

Figure 18. Schematic drawings of the pneumatic capacitor

of the pressurization waveform. Figure 18 illustrates the pneumatic capacitor with engineering drawings. The pneumatic capacitor consisted of a rigid cylinder of adjustable volume with a dome cap supporting a flexible membrane. This membrane allowed air to collect and eject during each inflation cycle, thus attenuating the rapid initial pressurization of the EHI seen with the regular driveline. The capacitor permitted a slightly longer ID (effectively AD) due to the slower inflation rate, in addition to a higher tank pressure; an extended AD was the priority here to examine the effect of longer assist.

4.2.4. Driver V3: Series Activation of Pneumatic Disks

The Series Driver featured pneumatic isolator disks designed to activate in series – in contrast to V1 with 3 pneumatic isolator disks that activate in parallel. Two separate Driver control computers allowed each pneumatic isolator disk stage to be activated independently. To facilitate synchronized triggering, the trigger signal from the IVY 7700 Patient Monitor was bifurcated to two separate Driver circuit board configurations. One set of electrical controls (Driver 1) controlled a single pneumatic isolator intended to activate during IVC, and the other set of electrical controls (Driver 2) were dedicated to a pair of pneumatic isolators coupled in parallel, designed to activate during the ejection phase of systole.

Both drivers in this system shared the same Isolator Input space, controlled by a single Pressure valve, a single Vacuum valve, and a single Vent valve. Each driver in the system had its own Inflate, Refill, Deflate, and Equalize valves; however, the only valves that did not open in synchrony were the Inflate valves. The inflate valves did, however, close in synchrony so long as both driver Assist Durations (TAD + ID) were equal. The

activation timing of each stage (TAD1 and TAD2) is illustrated in Figure 19 and the pneumatic hardware setup for this Driver is summarized schematically in Figure 20.

4.2.5. In vivo Study Methods

Two (2) separate acute ovine, non-GLP studies were conducted for this investigation. Each study utilized a single, anesthetized adult domestic cross ovine (62-78 kg). The *in vivo* study methods, including surgical approach, device implantation, and acute failure model for this investigation are identical to those described in Section 4.2.2. All experiments were conducted under an Animal Use Protocol (AUP) that was approved by the Texas A&M University Institutional Animal Care and Use Committee (IACUC) or the Texas Heart Institute IACUC.

4.2.6. Data Collection and Statistical Analysis

ADInstruments PowerLab data acquisition hardware and LabChart software were used to continuously record all physiologic parameters and EpicHeart™ data. All physiological pressures and flows were obtained using the methods described in Section 4.2.2. Paired samples of 10-20 seconds of device standby and successive device assist were collected for analysis. The data population over 2 animals consisted of 10 paired samples of 10-20s of data. The samples were averaged over the selection using LabChart, and then averaged in Microsoft Excel to provide overall results for each Driver version. Standard deviations are representative of variations amongst data runs for each animal.

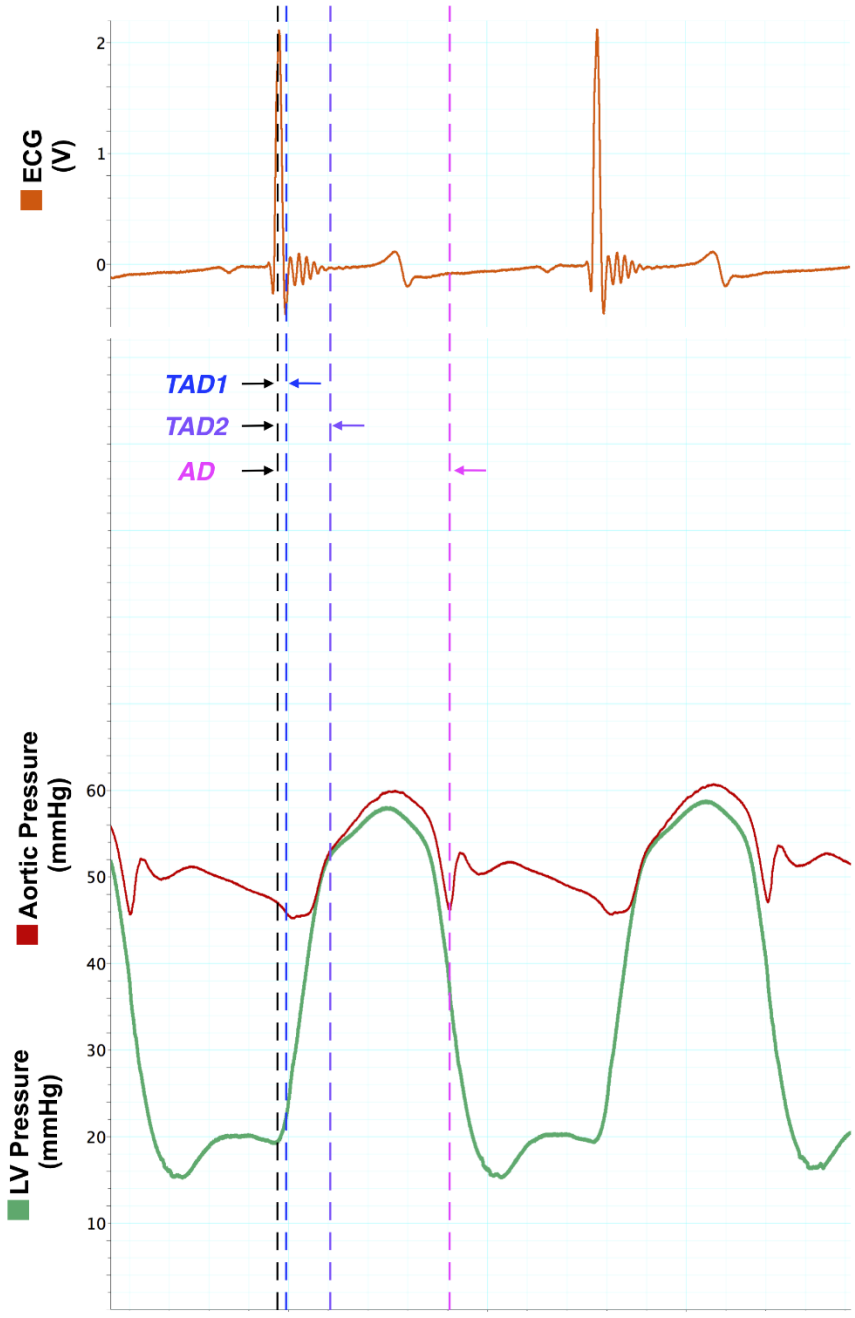

Figure 19. Waveform demonstration of the TAD1 and TAD2 parameters for the Series Driver (V3)

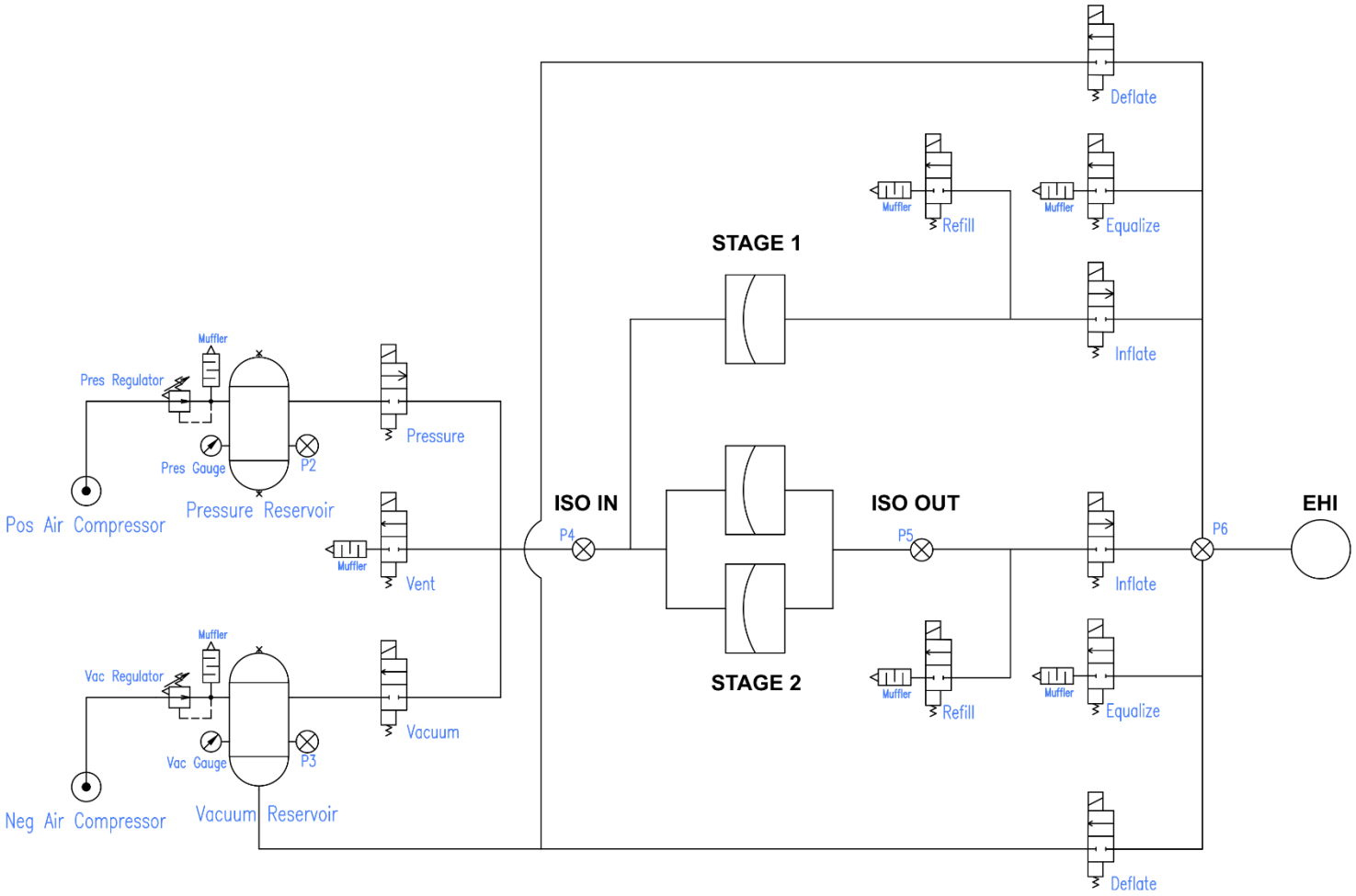

Figure 20. Pneumatic hardware schematic of the Series Driver; P1-6 are pressure transducers; each solenoid valve is labeled by name, Pressure, Vent, Vacuum, Refill, Inflate, Equalize, and Deflate; the ISO IN and ISO OUT label the input and output side of the pneumatic isolator disks; STAGE 1 was activated with cardiac IVC and was controlled by one computer, while STAGE 2 was activated during cardiac ejection and was controlled by a second computer

4.3. Results

4.3.1. Regular vs. Capacitor Driveline, Acute Failure

When the driveline pneumatic capacitor was included with Driver operation, there was some improvement to device assist. The Driver with the regular driveline could not operate with an assist duration above 125 ms and a reservoir pressure of 100 mmHg without compromising Implantable prototype integrity. However, the Driver with the pneumatic capacitor in the driveline permitted a slightly longer assist duration of 150 ms, and a higher reservoir pressure of 150 mmHg. Additionally, the average systolic assist pressure with the regular driveline was only 19 mmHg, but increased to 23 mmHg with the higher reservoir pressure used for the pneumatic capacitor driveline.

This application of increased epicardial assist during acute esmolol-induced failure conditions resulted in some improvement to cardiac pump function hemodynamics (Figure 21). Assist with the regular driveline resulted in a 0.8 L/min improvement in CO, however assist with the pneumatic capacitor resulted in a 1.1 L/min increase in CO. Similarly, the increase in SV improved with the inclusion of the pneumatic capacitor – a 14 mL increase versus only a 10 mL increase in SV. Additionally, the increase in LVSW with the regular driveline was 113%, and was even better at 163% with the pneumatic capacitor driveline.

The majority of the hemodynamic pressures – specifically SBP, PASP, PADP, and PAMP – resulted in similar changes with both versions of the Parallel Driver (Figure 22). However, there were differing effects on the MAP and DBP between the two versions of the Driver; while the DBP increased by 3 mmHg with the regular driveline, it actually

decreased by 6 mmHg with the capacitor driveline, resulting in a lower MAP during assist. Finally, assist with both Drivers lead to an increase in the mean CVP. This change was much greater with the capacitor driveline, an increase of 5 mmHg versus an increase of only 1 mmHg.

Assist during acute esmolol-induced failure with each version of the pneumatic driveline resulted in mostly comparable hemodynamic waveforms (Figure 23). One slight difference was the transition between the Inflate Duration and the closing of the Inflate solenoid valve. Assist with the capacitor driveline had a smoother transition when the Inflate solenoid valve closed, opposed to the abrupt change with the regular driveline. Notice that the LVP and AoP experience a slight decrease in pressure at this moment, before increasing again with ascending ejection.

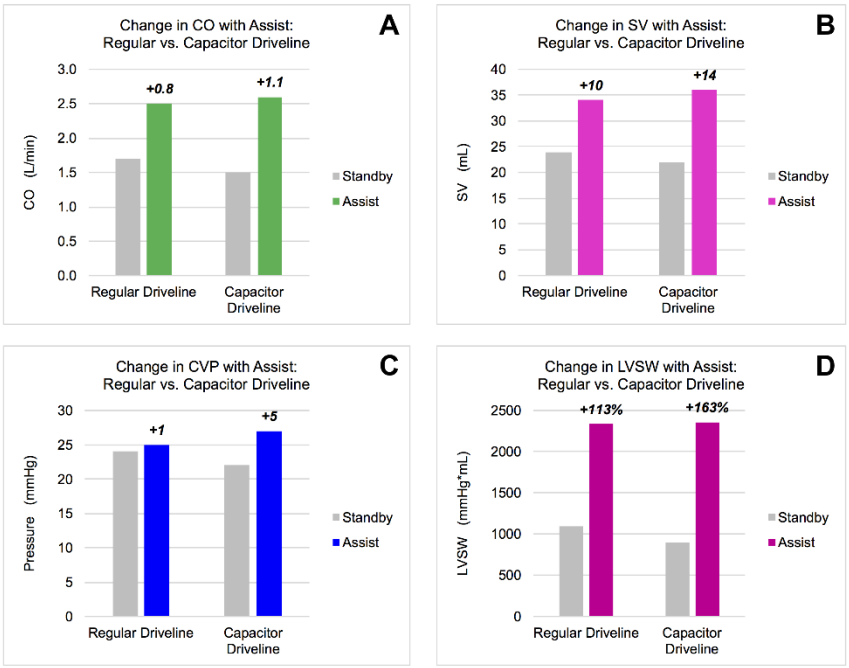

Figure 21. Changes in cardiac pump function (CO, LVSV, LVSW) and CVP during assist with the Parallel Driver using the regular driveline and the pneumatic capacitor driveline

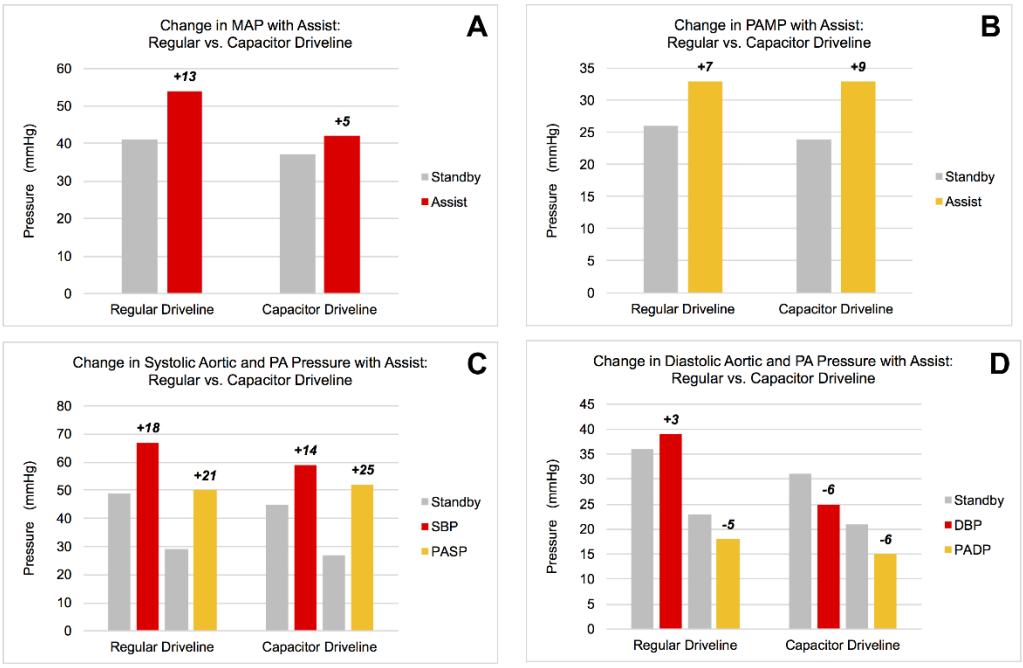

Figure 22. Changes in aortic and pulmonary pressures during assist with the Parallel Driver using the regular driveline and the pneumatic capacitor driveline

4.3.2. Parallel vs. Series Activation of Pneumatic Disks, Baseline Heart

The next group of results compare the activation of three pneumatic disks in parallel with the pneumatic capacitor driveline, versus activation of the pneumatic disks in series (without a driveline capacitor). With the Series Driver, a single disk was activated during IVC, following by a delayed activation of the remaining two disks, timed to activate during ejection.

Prior to the start of esmolol-induced acute failure, both Drivers were operated to evaluate the effect on the baseline heart. Comparable changes were observed in the hemodynamic waveforms, and in almost all quantitatively measured hemodynamic parameters (see Figure 24 for hemodynamic waveform comparison). The changes in CO,

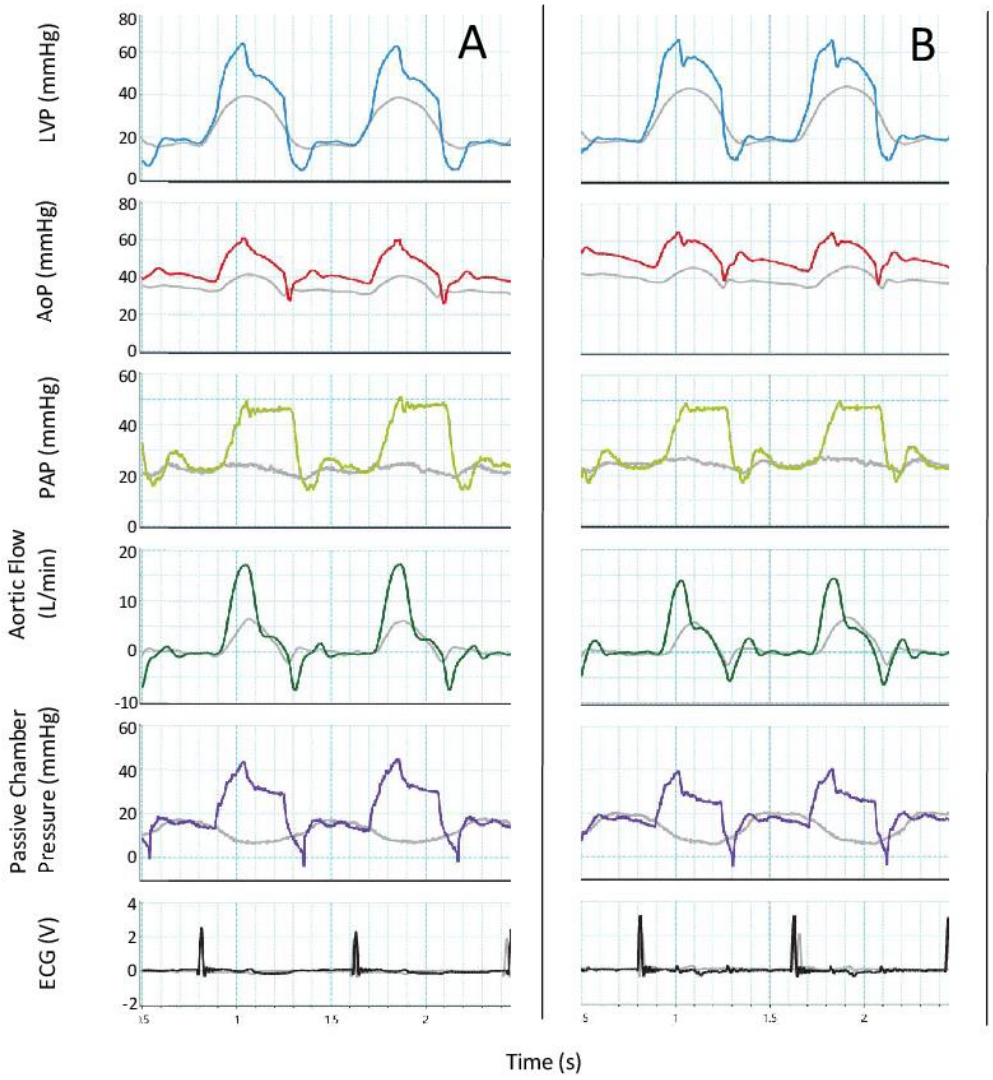

Figure 23. Hemodynamic waveform comparison between assist with the capacitor driveline (A), and the regular driveline (B) using the Parallel Driver; all gray waveforms represent standby, while the saturated colors reveal assist waveforms

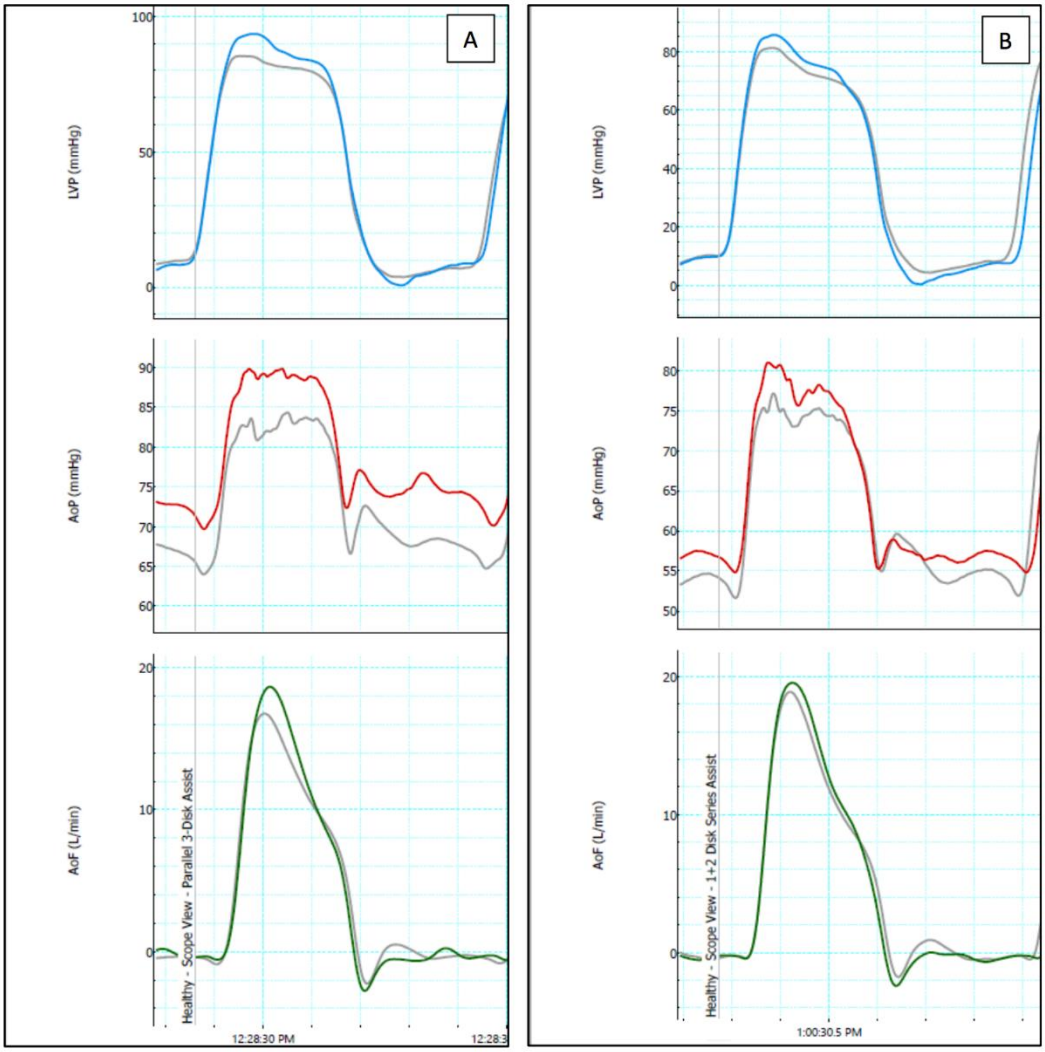

Figure 24. Physiologic signals to demonstrate change in LVP (blue), AoP (red), and AoF (green) with device assist during baseline conditions; (A) Standby and Assist conditions with the Parallel Driver; (B) Standby and Assist conditions with the Series Driver; note that neither driver shows a negative impact on normal physiologic profile of each physiologic parameter – only an increase in instantaneous magnitude; for both (A) and (B), the foreground saturated colors (Blue, Red, Green) represent the assist conditions, and the gray represent the corresponding standby conditions (sampled less than 1 min prior to each assist sample)

SV, PASP, PADP, PAMP, and CVP with assist using each Driver were nearly equivalent (Table 5). The only notable difference in assist was the change in AoP; the parallel driver with the capacitor driveline had a higher reservoir pressure (150 mmHg vs. 60 mmHg), and thus a higher mean systolic assist pressure (7 mmHg vs. 4 mmHg). This resulted in a slightly greater increase in SBP, DBP, and MAP with the parallel Driver (Table 5). Similarly, the increase in LVSW with assist was slightly more pronounced with the parallel Driver than the series Driver (Table 5).

Table 5. Summary of changes in hemodynamic parameters with assist during baseline conditions using the Parallel Driver and the Series Driver

	PARALLEL DRIVER			**SERIES DRIVER**		
	Standby	Assist	Δ	Standby	Assist	Δ
SBP (mmHg)	79	89	**10**	80	85	**5**
DBP (mmHg)	59	68	**9**	60	63	**3**
MAP (mmHg)	68	76	**8**	69	72	**3**
PASP (mmHg)	17	16	**-1**	17	16	**-1**
PADP (mmHg)	8	7	**-1**	9	8	**-1**
PAMP (mmHg)	13	11	**-2**	13	12	**-1**
CVP (mmHg)	6	6	**0**	5	5	**0**
LV EDP (mmHg)	8	7	**-1**	8	7	**-1**
LV SV (mL)	38	41	**3**	40	43	**3**
CO (L/min)	3.9	4.1	**0.2**	4.3	4.5	**0.2**
LV SW (mmHg*mL)	2874	3669	**795**	3089	3543	**454**
EHDP		7			4	

4.3.3. Parallel vs. Series Activation of Pneumatic Disks, Acute Failure

Activation with each Driver resulted in the same increase in CO (+1.1 L/min) and SV (+13 mL) during acute heart failure, however the series driver resulted in more physiologic hemodynamic waveforms, compared to the parallel driver with a pneumatic capacitor. This improvement to hemodynamic waveforms is shown in Figure 25.

In addition to maintaining physiologic hemodynamics, assist with the series driver led to better arterial pressure results during acute heart failure. While both Drivers resulted in a similar increase in aortic pressures, the change in pulmonary pressure was more ideal with the series driver. Specifically, the parallel driver caused a 25 mmHg increase in the PASP, where the series driver resulted in a 4 mmHg increase. This is related to the change in PAMP, which increased by 9 mmHg with the parallel driver, and only 1 mmHg with the series driver. When considering the diastolic pressures, the changes with the parallel driver were dissimilar to the series driver; the DBP and the PADP both decreased by 6 mmHg during assist with the parallel driver. In contrast, the DBP increased by 2 mmHg, and the PADP decreased by only 1 mmHg with the series driver. Finally, while assist with the series driver resulted in a 1 mmHg increase in mean CVP, assist with the parallel driver increased the mean CVP by 6 mmHg. These results are summarized graphically in Figure 26 and Figure 27.

4.3.4. Parallel vs. Series Activation of Pneumatic Disks, Extreme Failure

The parallel driver and the series driver were directly compared during extreme failure conditions, defined by a CO of <1 L/min during device standby. Once again, the relative change in CO was comparable – a 1.1 L/min increase for the parallel driver and a

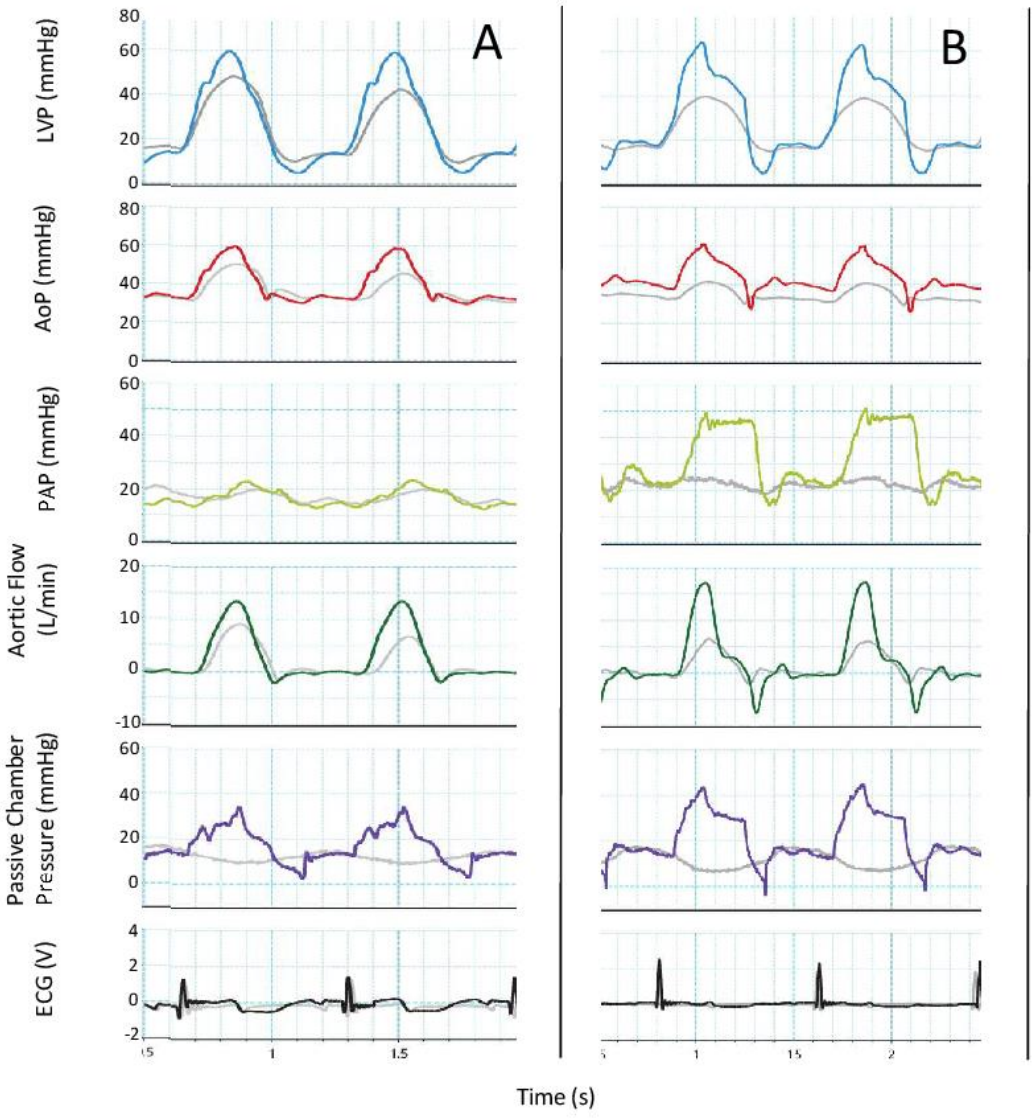

Figure 25. Hemodynamic waveform comparison between assist with the Series Driver (A) and assist with the Parallel Driver during acute failure (B); notice the improved hemodynamics, particularly with the PAP and the aortic flow; for both (A) and (B), the foreground saturated colors (Blue, Red, Yellow, Green, Purple, and Black) represent the assist conditions, and the gray represent the corresponding standby conditions (sampled less than 1 min prior to each assist sample)

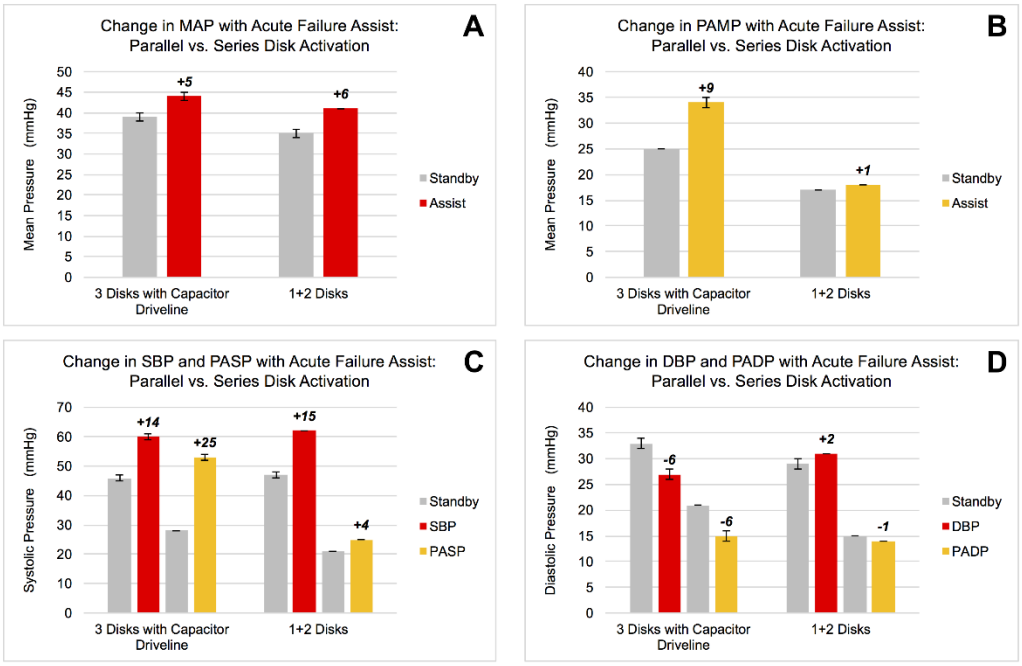

Figure 26. Changes in aortic and pulmonary pressures during assist with the Parallel Driver using the pneumatic capacitor driveline compared to the Series Driver

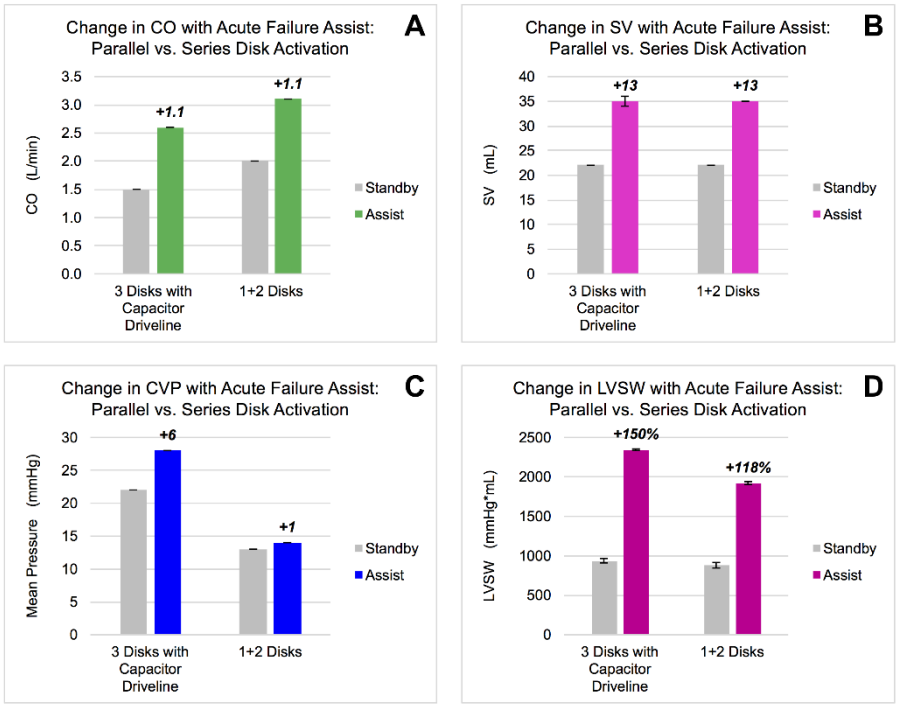

Figure 27. Changes in cardiac pump function (CO, LVSV, LVSW) and CVP during assist with the Parallel Driver using the pneumatic capacitor driveline compared to the Series Driver

1.2 L/min increase for the series driver. Additionally, the changes in MAP and PAMP were also similar for assist with each driver. However once again, the series driver provided assist with more physiologic hemodynamics than the parallel driver. These results are summarized in Table 6 and Figure 28.

Table 6. Summary of changes in hemodynamic parameters with assist during extreme failure conditions using the Parallel Driver and the Series Driver

	PARALLEL DRIVER			**SERIES DRIVER**		
	Standby	Assist	Δ	Standby	Assist	Δ
SBP (mmHg)	30	48	**18**	31	48	**17**
DBP (mmHg)	21	14	**-7**	19	19	**0**
MAP (mmHg)	23	28	**5**	23	30	**7**
PASP (mmHg)	21	26	**5**	19	21	**2**
PADP (mmHg)	18	15	**-3**	13	12	**-1**
PAMP (mmHg)	19	20	**1**	15	16	**1**
CVP (mmHg)	18	20	**2**	13	16	**3**
LV EDP (mmHg)	19	19	**0**	14	14	**0**
LV SV (mL)	4	21	**17**	9	21	**12**
CO (L/min)	0.3	1.4	**1.1**	0.7	1.9	**1.2**
LV SW (mmHg*mL)	93	752	**659**	216	932	**716**
EHDP		15			20	

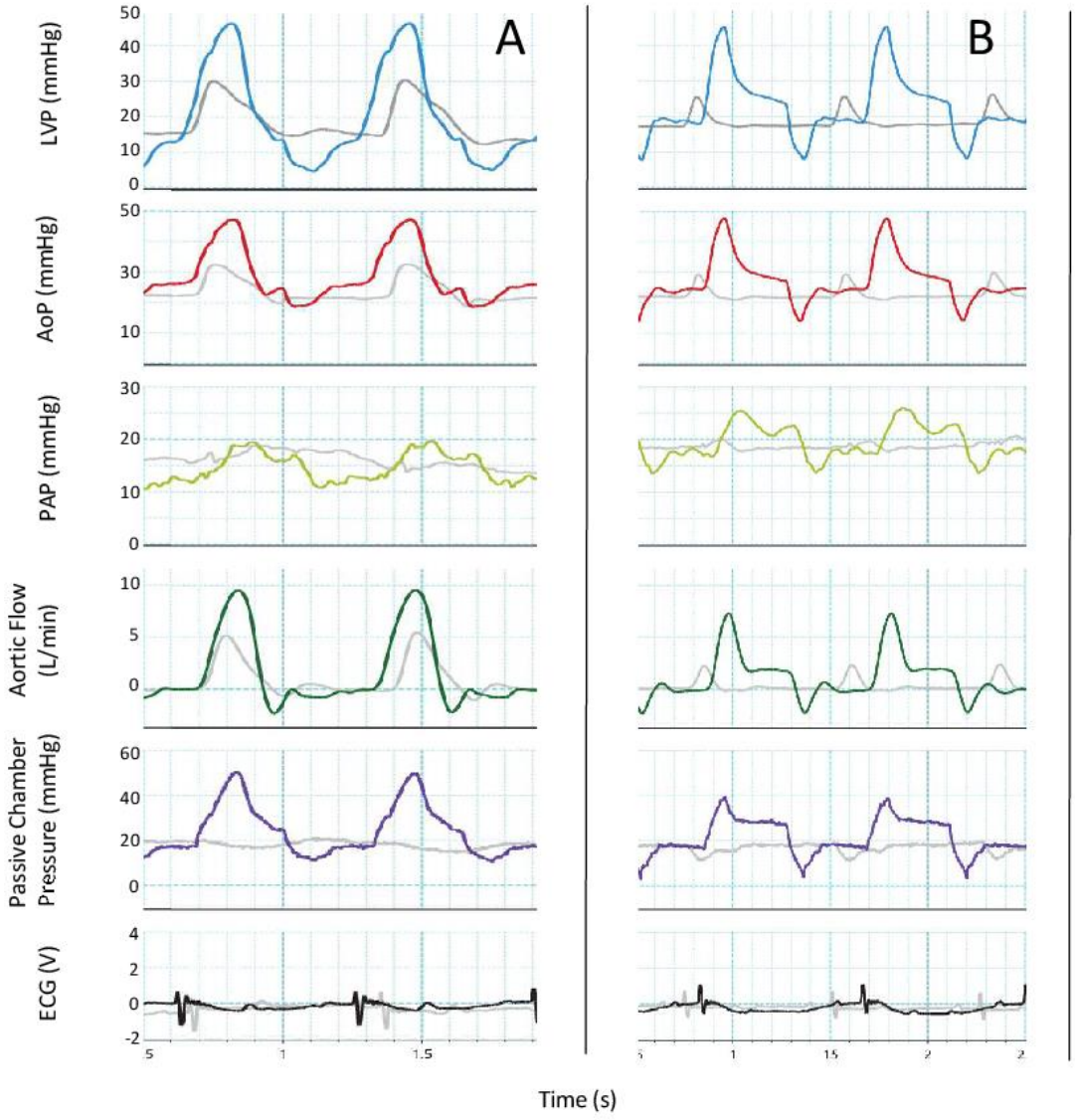

Figure 28. Hemodynamic waveform comparison between assist with the Series Driver (A) and assist with the Parallel Driver (B) during extreme failure conditions; notice the improved hemodynamics, particularly with the LVP, AoP, and the aortic flow; for both (A) and (B), the foreground saturated colors (Blue, Red, Yellow, Green, Purple, and Black) represent the assist conditions, and the gray represent the corresponding standby conditions (sampled less than 1 min prior to each assist sample)

4.4. Discussion

This study was an investigation of methods for synchronizing device pressurization with heart contraction for the purpose of optimizing epicardial compressive assist on the acutely failing heart. The methods for exploring synchrony with LV pressurization included adjustments to the Driver control software and hardware, with methods verified in two ovine acute heart failure model *in vivo* studies.

While the introduction of a pneumatic capacitor resulted in slight improvements to the CO over the original Driveline, the most noteworthy outcomes of this investigation were the resulting hemodynamics during assist with the Series Driver. Although it was expected that pressurization timing and rate would match IVC with Driver updates, achieving such remarkable similarity to physiologic hemodynamics was surprising.

Other groups have reported methods of customizable DCC assist. First, Hotei et al reported using a %Systole parameter to adjust the duration and onset timing of LV assist in a canine LV failure model.[19] Their model was NaOH injection into the LV free wall myocardium to induce necrosis; the device was sutured over the region of necrotic tissue. They activated their device with no delay (no delay of activation from R-wave trigger) and a duration that was 40% of the RR interval (full systole), as well as limiting assist to the first 20% of RR (early systole assist) and delaying assist by 20% of RR (late systole assist). It is interesting to note that they observed the greatest efficacy when assist was delayed by 20% of the RR interval, as this can be compared to the second stage of pneumatic disk activation with the Series Driver, or assist during ejection. The Hotei group reported significant assist during IVC (as indicated by increases in peak LV dP/dt)

with early systole activation and minimal effect with late systole activation; in contrast, they observed the greatest increase in CO with assist during late systole, and minimal change with assist limited to early systole. The results of our study show that by combining the epicardial compression into two phases, heart assist is optimized. Additionally, it is hypothesized that as the heart recovers, assist may only be needed with IVC, and for this reason, customizable stages of assist are favorable.

More recently, the Roche et al group reported an updated DCC device that is designed to combine circumferential compression with active twisting.[12] Although they describe a highly customizable pneumatic pressure control system and report comparable increases in CO to the present study results, the aortic flow waveforms appear to deviate significantly from the baseline hemodynamics.

Efficacy of the driver was the focus of this study, yet practical considerations were also utilized in driver design. Specifically, the capacitor component was added to smooth the pressure spike created by the parallel driver configuration, and then the series driver was developed to obtain a more uniform pressurization during systole without the need for the capacitor component. It is desirable to eliminate the capacitor component with a software change because a system with fewer components is potentially more robust.

4.4.1. Study Limitations

While the data from the sections reporting a comparison of the Parallel Driver to the Series Driver under baseline conditions and extreme failure conditions are from the same animal, the results during normal acute failure conditions are from two separate animal studies. It is possible that comparisons here are limited by variations in animal

response to esmolol and slight variations in the construction of the EpicHeart™ Implantable (EHI) between the two animals. There were no studies during which the parallel and series drivers were both operated under normal failure conditions, as an unexpected animal response to high dose of esmolol occurred in the study intended to compare these two versions of the Driver. However, the samples compared are from as similar as possible failure conditions, and equal reservoir pressure settings.

Additionally, sample sizes for this investigation were limited by having multiple study aims in the protocol, as well as various unforeseen study complications. A significant amount of time was devoted to assessing assist on the healthy heart as a result of updates to the EHI between studies. While the resulting increases in cardiac performance and physiologic waveforms on the healthy heart were remarkable, the time devoted to this study aim limited the amount of time devoted to other study aims.

One limitation of the Driver is the numerous user-defined parameters, as they introduce risk of operator error; for example, there is no feedback between the ECG QT duration (systole) and the driver software. Because of this, the user is responsible for measuring systole and determining a proper systolic duration, and properly updating the corresponding driver parameter. Finally, while the increased assist duration (AD) improved the CO, this parameter limited the maximum operational rate of assist; as the TAD+ID was increased (AD), the maximum sustainable HR decreased. If the animal was tachycardic, the AD may be limited to a value below the ideal assist duration. Efforts will be made to optimize the system to accommodate higher heart rates, as many heart failure patients are commonly tachycardic.

4.5. Conclusion

The results of this study show that not only does the EpicHeart™ Device assist the heart during acute failure, but that it can be done in a manner that mimics the innate cardiac pressurization and hemodynamics. This element of direct cardiac compression assist is vital to encouraging healthy growth and remodeling, and potentially bridge-to-recovery.

5. SUMMARY

In summary, an innovative heart assist technology currently under investigation has been presented for potential use in heart failure therapy. Proof-of-concept studies completed prior to this work were encouraging, but lacked repeated results, justifying the need for additional acute studies. The results of these additional studies were reported here, and show a 75% recovery of baseline CO, on average. This demonstrates the efficacy of the device to provide an increase in the CO during acute heart failure. Still, questions remain regarding the efficacy of the device over longer durations, as well as in chronic heart failure conditions. These questions will be the topic of future investigations.

The *in vivo* studies for evaluation of device efficacy were coupled with the development of a device simulation tool. A validated simulation of the device will be invaluable when transitioning from preclinical animal models to human trials. The simulation data analyzed here for verification of performance specifications revealed minimal variation between *in vivo* and simulated hemodynamic effects of device assist. As this was a pilot study, more studies are needed to investigate the simulation parameters considered beyond the scope of this work. Optimistically, this simulation tool will provide clinical professionals with insight regarding which patients will benefit the most from therapy with this epicardial heart assist device.

The knowledge gained from this study will guide future development of the device, with the ultimate goal of device therapy for heart recovery.

REFERENCES

1. Benjamin EJ, Blaha MJ, Chiuve SE, Cushman M, Das SR, *et al*: Heart Disease and Stroke Statistics—2017 Update: A Report from the American Heart Association. *Circulation*, 2017 doi: 10.1161/cir.0000000000000485.
2. Baig MK, Mahon N, McKenna WJ, Caforio AL, Bonow RO, *et al*: The Pathophysiology of Advanced Heart Failure. *Heart & Lung : The Journal of Critical Care* 28 (2): 87-101, 1999 doi: 10.1053/hl.1999.v28.a97762.
3. Louridas GE, Lourida KG: Systems Biology and Biomechanical Model of Heart Failure. *Curr Cardiol Rev* 8 (3): 220-30, 2012.
4. Mann DL: The Evolution of Modern Theory and Therapy for Heart Failure. *Progress in Pediatric Cardiology* 37 (1-2): 9-12, 2014 doi: 10.1016/j.ppedcard.2014.10.002.
5. Mann DL, Bristow MR: Mechanisms and Models in Heart Failure: The Biomechanical Model and Beyond. *Circulation* 111 (21): 2837-49, 2005 doi: 10.1161/CIRCULATIONAHA.104.500546.
6. Poppas A, Rounds S: Congestive Heart Failure. *Am J Respir Crit Care Med* 165 (1): 4-8, 2002 doi: 10.1164/ajrccm.165.1.2102075.
7. Merlo M, Pivetta A, Pinamonti B, Stolfo D, Zecchin M, *et al*: Long-Term Prognostic Impact of Therapeutic Strategies in Patients with Idiopathic Dilated Cardiomyopathy: Changing Mortality Over the Last 30 Years. *European Journal of Heart Failure* 16 (3): 317-324, 2014 doi: 10.1002/ejhf.16.

8. Lund LH, Edwards LB, Dipchand AI, Goldfarb S, Kucheryavaya AY, *et al*: The Registry of the International Society for Heart and Lung Transplantation: Thirty-Third Adult Heart Transplantation Report-2016; Focus Theme: Primary Diagnostic Indications for Transplant. *J Heart Lung Transplant* 35 (10): 1158-1169, 2016 doi: 10.1016/j.healun.2016.08.017.

9. Alraies MC, Eckman P: Adult Heart Transplant: Indications and Outcomes. *Journal of Thoracic Disease* 6 (8): 1120-1128, 2014 doi: 10.3978/j.issn.2072-1439.2014.06.44.

10. Moreno MR, Biswas S, Harrison LD, Miller MW, Nelson DA, *et al*: Assessment of Minimally Invasive Device That Provides Simultaneous Adjustable Cardiac Support and Active Synchronous Assist in an Acute Heart Failure Model. *Journal of Medical Devices* 5 (4): 041008-041008, 2011 doi: 10.1115/1.4004652.

11. Moreno MR, Biswas S, Harrison LD, Miller MW, Nelson DA, *et al*: Development of a Non-Blood Contacting Cardiac Assist and Support Device: An in Vivo Proof of Concept Study. *Journal of Medical Devices* 5 (4): 041007-041007, 2011 doi: 10.1115/1.4005281.

12. Roche ET, Horvath MA, Wamala I, Alazmani A, Song SE, *et al*: Soft Robotic Sleeve Supports Heart Function. *Science Translational Medicine* 9 (373), 2017 doi: 10.1126/scitranslmed.aaf3925.

13. Abraham WT, Aggarwal S, Prabhu SD, Cecere R, Pamboukian SV, *et al*: Ambulatory Extra-Aortic Counterpulsation in Patients with Moderate to Severe

Chronic Heart Failure. *JACC Heart Fail* 2 (5): 526-33, 2014 doi: 10.1016/j.jchf.2014.04.014.

14. Cohn WE, Winkler JA, Tuzun E, Hjelle A, Bassett K, *et al*: Contrast Pericardiography Facilitates Intrapericardial Navigation under Fluoroscopy. *Ann Thorac Surg* 90 (5): 1537-40, 2010 doi: 10.1016/j.athoracsur.2010.06.025.
15. Jaillon P, Drici M: Recent Antiarrhythmic Drugs. *Am J Cardiol* 64 (20): 65J-69J, 1989.
16. Burkhoff D, Maurer MS, Joseph SM, Rogers JG, Birati EY, *et al*: Left Atrial Decompression Pump for Severe Heart Failure with Preserved Ejection Fraction: Theoretical and Clinical Considerations. *JACC Heart Fail* 3 (4): 275-82, 2015 doi: 10.1016/j.jchf.2014.10.011.
17. Kaye D, Shah SJ, Borlaug BA, Gustafsson F, Komtebedde J, *et al*: Effects of an Interatrial Shunt on Rest and Exercise Hemodynamics: Results of a Computer Simulation in Heart Failure. *Journal of Cardiac Failure* 20 (3): 212-21, 2014 doi: 10.1016/j.cardfail.2014.01.005.
18. Punnoose L, Burkhoff D, Rich S, Horn EM: Right Ventricular Assist Device in End-Stage Pulmonary Arterial Hypertension: Insights from a Computational Model of the Cardiovascular System. *Progress in Cardiovascular Diseases* 55 (2): 234-243 e2, 2012 doi: 10.1016/j.pcad.2012.07.008.
19. Hotei H, Koura Y, Orihashi K, Sueda T, Fukunaga S, Matsuura Y: Development of a Direct Mechanical Left Ventricular Assist Device for Left Ventricular Failure. *Artif Organs* 21 (9): 1026-34, 1997.

APPENDIX

Table A 1. Summary of *in vivo* sources for each Patient Simulator input

PARAMETER	STUDY 1	STUDY 2	STUDY 3	STUDY 4
HR	Rate of Dual P Millar	Rate of Dual P Millar	Rate of Dual P Millar	Rate of Dual P Millar
EF	AoF Probe (CO) & RVEDV	AoF Probe (CO) & RVEDV	AoF Probe (CO) & RVEDV	AoF Probe (CO) & RVEDV
TH	CT Data - Constant	CT Data - Constant	CT Data - Constant	CT Data - Constant
CO	Ao Flow Probe	Ao Flow Probe	Ao Flow Probe	Ao Flow Probe
CVP	Swan-Ganz	Swan-Ganz	Swan-Ganz	Swan-Ganz
PAP S/D	Swan-Ganz	Swan-Ganz	Estimated	Estimated
PAPM	Swan-Ganz	Swan-Ganz	Estimated	Estimated
PCWP	use LVP EDP (Millar)	use LVP EDP (Millar)	use LVP EDP (Millar)	use LVP EDP (Millar)
AOP S/D	Dual P Millar	Dual P Millar	Dual P Millar	Dual P Millar
AOPM	Dual P Millar	Dual P Millar	Dual P Millar	Dual P Millar
RA EDV	CT Data - Constant	CT Data - Constant	CT Data - Constant	CT Data - Constant
LA EDV	CT Data - Constant	CT Data - Constant	CT Data - Constant	CT Data - Constant
RV EDV	CT Data - Constant	CT Data - Constant	CT Data - Constant	CT Data - Constant

Table A 2. Summary of hemodynamic outputs evaluated during this pilot investigation of the Harvi-CorInnova simulation application

OUTPUT	STUDY 1	STUDY 2	STUDY 3	STUDY 4
AoP s/d/m	Dual P Millar	Dual P Millar	Dual P Millar	Dual P Millar
PAP s/d/m	Swan-Ganz	Swan-Ganz	Estimated	Estimated
LAP s/d/m	*exclude from analysis*	*exclude from analysis*	*exclude from analysis*	*exclude from analysis*
RAP s/d/m	*exclude from analysis*	*exclude from analysis*	*exclude from analysis*	*exclude from analysis*
PWP	use LVP EDP	use LVP EDP	use LVP EDP	use LVP EDP
CVP	Swan-Ganz	Swan-Ganz	Swan-Ganz	Swan-Ganz
EDV LV/RV	*exclude from analysis*	*exclude from analysis*	*exclude from analysis*	*exclude from analysis*
EDP LV/RV	LV only - Dual P Millar	LV only - Dual P Millar	LV only - Dual P Millar	LV only - Dual P Millar
ESV LV/RV	*exclude from analysis*	*exclude from analysis*	*exclude from analysis*	*exclude from analysis*
ESP LV/RV	*exclude from analysis*	*exclude from analysis*	*exclude from analysis*	*exclude from analysis*
SV LV/RV	LV only - flow probe	LV only - flow probe	LV only - flow probe	LV only - flow probe
CO LV/RV	LV only - flow probe	LV only - flow probe	LV only - flow probe	LV only - flow probe
SW LV/RV	LV – flow probe/Millar	LV – flow probe/Millar	LV – flow probe/Millar	LV – flow probe/Millar
CPO LV/RV	LV – flow probe/Millar	LV – flow probe/Millar	LV – flow probe/Millar	LV – flow probe/Millar

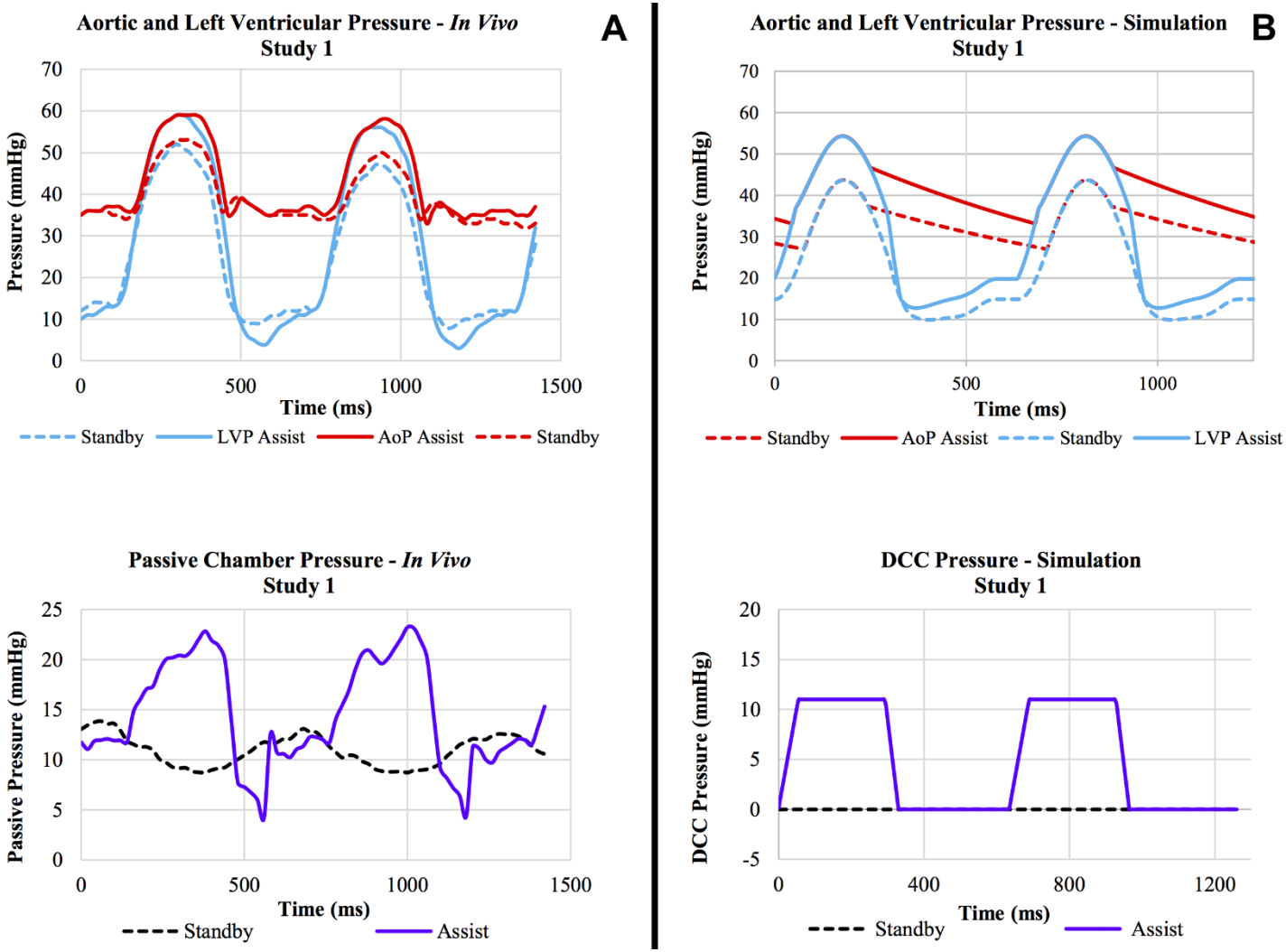

Figure A 1. Hemodynamic waveform comparison between *in vivo* (A) and simulation assist (B); figure shows left heart pressures (LVP and AoP) as well as DCC assist pressure *in vivo* and in simulation

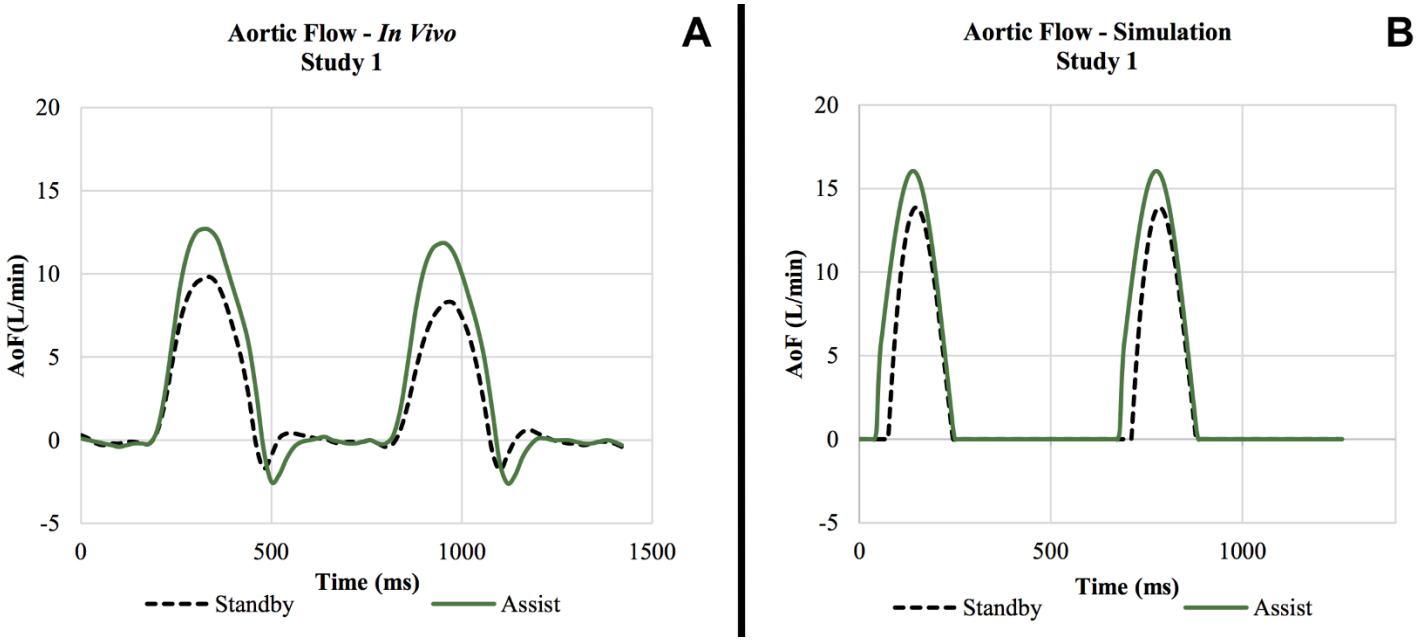

Figure A 2. Hemodynamic waveform comparison between *in vivo* aortic flow (A) and simulated aortic flow (B); both device standby and device assist conditions are plotted